Fossil Record 28 (2) 2025, 321–346 | DOI 10.3897/fr.28.167846

PENSOFT

MUSEUM FÜR NATURKUNDE BERLIN

New dwarf crocodylomorph from the Upper Jurassic of Portugal and the first neuroanatomical data for Atoposauridae

E. Puértolas-Pascual[1,2,3*]

1 *Grupo Aragosaurus-IUCA, Paleontología, Facultad de Ciencias, Universidad de Zaragoza, C/Pedro Cerbuna, 12, 50009 Zaragoza, (Zaragoza), Spain*

2 *GeoBioTec, Departamento de Ciências da Terra FCT, Universidade Nova de Lisboa, 2829-516 Campus Monte de Caparica, (Caparica), Portugal*

3 *Museu da Lourinhã, Rua João Luis de Moura, 95, 2530-158 Lourinhã, (Lisboa), Portugal*

https://zoobank.org/FA2E32F7-FE35-4475-B5CF-05BFC1D6101B

Corresponding author: E. Puértolas-Pascual (eduardo.puertolas@gmail.com)

Academic editor: Florian Witzmann ♦ **Received** 5 August 2025 ♦ **Accepted** 4 October 2025 ♦ **Published** 27 October 2025

Abstract

A new crocodylomorph fossil specimen (ML2631) from the Upper Jurassic of Lourinhã (Portugal) is described, based on a partially preserved skull table and braincase. The specimen was recovered from the Zimbral vertebrate microfossil assemblage, located in the lower part of the Praia Azul Member of the Lourinhã Formation (Kimmeridgian–Tithonian transition). The fossil was scanned using high-resolution micro-computed tomography (μCT), enabling the digital reconstruction of internal cranial structures, such as the brain cavity, cranial nerves, inner ear and paratympanic sinus system. These reconstructions represent the first neuroanatomical data ever reported for Atoposauridae, a clade of small-bodied neosuchian crocodylomorphs common in the Late Jurassic and Cretaceous of Europe.

Phylogenetic analysis places ML2631 within Atoposauridae and contributes to resolving previously uncertain relationships within the group. Although fragmentary, ML2631 exhibits a unique combination of anatomical features, including a dorsolaterally open cranioquadrate passage, a sagittal crest along the frontal and parietal, a large, posteriorly placed and septate choana, large supratemporal fenestrae with a distinct posterior fossa and a squamosal lobe bearing a discontinuous lateral groove. These traits, amongst others, distinguish ML2631 from all other known atoposaurid species. Additionally, its neuroanatomical proportions suggest a dwarf adult individual with low-frequency auditory sensitivity and moderate visual acuity, consistent with a primarily terrestrial or nearshore lifestyle, coherent with the depositional environment of the fossil site. Taken together, these results highlight the taxonomic and evolutionary relevance of the specimen and underline the importance of future discoveries of more complete material to confirm its systematic and phylogenetic status within Atoposauridae.

Key Words

Crocodylomorpha, Kimmeridgian-Tithonian, Lourinhã Formation, Neosuchia, Portugal, Upper Jurassic

Introduction

The Lourinhã Formation (Late Jurassic, Kimmeridgian–Tithonian) of western Portugal is internationally recognised for its rich and diverse fossil record, which ranks amongst the most significant of its age in Europe. Deposited within the Lusitanian Basin (Fig. 1), this formation includes a variety of fluvial and transitional to marine facies that have yielded exceptionally well-preserved remains of vertebrates including dinosaurs (e.g. Mateus et al. (2017); Costa and Mateus (2019); Rotatori et al. (2022); amphibians and lepidosaurs (Guillaume et al. (2022); Guillaume (2024)); mammals (Guillaume (2024)); turtles (Pérez-García and Ortega (2011));

* No current institutional affiliation, collaborator of 1, 2, 3.

pterosaurs (Fernandes et al. (2023)); fishes (Guillaume (2024)); and crocodylomorphs (see below). Amongst these, crocodylomorphs represent one of the most taxonomically and ecologically diverse components, with fossils recovered both from macrofossil sites and microvertebrate-rich layers.

Crocodylomorph remains from the Upper Jurassic of Portugal include taxa of various body sizes and ecological niches, ranging from large fully marine forms, such as *Machimosaurus* (Krebs 1967, 1968; Young et al. 2014), to small, more terrestrial taxa like atoposaurids, semi-aquatic species with durophagous feeding adaptations, such as bernissartiids and larger-bodied animals with more generalist feeding behaviour, such as goniopholidids (Guillaume et al. 2020). The famous Guimarota lignite mine, located further north in the Alcobaça Formation (Leiria, Portugal), produced an extraordinary assemblage of small vertebrates including the atoposaurid *Theriosuchus guimarotae* Schwarz & Salisbury, 2005, which was later re-assigned to the new genus *Knoetschkesuchus guimarotae* (Schwarz et al. 2017). This taxon represents one of the best-known atoposaurids from the Iberian Peninsula. Additionally, in Guimarota, *Goniopholis baryglyphaeus* Schwarz, 2002, a medium-sized goniopholidid and other enigmatic crocodylomorphs, such as *Lisboasaurus estesi* Seiffert, 1970 and *Lusitanisuchus mitracostatus* (Seiffert, 1970) were recovered. These two latter taxa were initially misidentified as anguimorph lizards (Seiffert 1970, 1973) or even theropod dinosaurs (Milner and Evans 1991), but were later re-assigned to Crocodylomorpha, based on new material and anatomical evidence (Buscalioni et al. 1996; Schwarz and Fechner 2004, 2008).

Within the Lourinhã Formation itself, several crocodylomorph taxa have been recognised in recent years. One of the most notable is *Ophiussasuchus paimogonectes* López-Rojas, Mateus, Marinheiro, Mateus & Puértolas-Pascual, 2024, a goniopholidid described from a nearly complete skull from Paimogo Beach (López-Rojas et al. 2024). In addition, postcranial material and isolated teeth from Valmitão, Peralta and other localities in the surroundings of Lourinhã have been attributed to several taxa, including *Lusitanisuchus*, Atoposauridae, Goniopholididae, Bernissartiidae and undetermined mesoeucrocodylians (Guillaume et al. 2020; Puértolas-Pascual and Mateus 2020). These discoveries suggest a higher taxonomic and ecological diversity of crocodylomorphs than previously assumed, based solely on macrofossils and more complete material.

Despite the diversity hinted at by the previously mentioned remains, the record of atoposaurids in the Lourinhã Formation remains poorly known. Most of the available material consists of fragmentary elements or isolated teeth recovered from microvertebrate assemblages (Guillaume et al. 2020), which limits detailed anatomical and phylogenetic interpretation. A partial skeleton including axial and appendicular elements from Baleal (near Peniche), tentatively assigned to *Knoetschkesuchus guimarotae*, was described by Eijkelboom (2020), but such finds remain exceptional. Nevertheless, atoposaurids represent a key group for understanding the evolution of Neosuchia, the early radiation of Eusuchia and the palaeobiogeographic history of Crocodylomorpha in the Late Jurassic of western Europe.

The present study provides new insights into this group, based on a new specimen from the coastal cliffs of Lourinhã: ML2631, a partial skull table and braincase preserved in a calcareous nodule (Fig. 3D) from the Zimbral site (Figs 1, 2). Since mechanical preparation could not expose all anatomical details, the specimen was scanned using micro-computed tomography (micro-CT), which enabled the digital reconstruction of several internal cranial cavities (Figs 3, 4). As a result, this study provides the first neuroanatomical data ever reported for the clade Atoposauridae. Prior to this work, the only crocodylomorph from Portugal for which neuroanatomical features had been described was *Portugalosuchus azenhae* Mateus, Puértolas-Pascual & Callapez, 2019, a eusuchian from the Cenomanian (Cretaceous) of Coimbra (Puértolas-Pascual et al. 2023). Previous digital neuroanatomical studies have proven useful for reconstructing sensory capabilities, brain morphology and palaeobiological traits in extinct crocodylomorphs, including representatives of Thalattosuchia (e.g. Brusatte et al. (2016); Pierce et al. (2017); Herrera et al. (2018)), Notosuchia (e.g. Sereno and Larsson (2009); Kley et al. (2010); Pochat-Cottilloux et al. (2022)), Tethysuchia (Erb and Turner 2021) and Eusuchia (e.g. Witmer et al. (2008); Kuzmin et al. (2021); Serrano-Martínez et al. (2021); Lessner and Holliday (2022)) amongst others. However, such data remain scarce for terrestrial Jurassic taxa and are entirely absent for atoposaurids.

Geological and geographical settings

The crocodylomorph specimen ML2631 was recovered from coastal outcrops in western Portugal, near the town of Lourinhã (Lisbon District, Oeste Region), where Upper Jurassic strata of the Lusitanian Basin are extensively exposed (Fig. 1). This sedimentary basin was formed through a multiphase rifting history along the western margin of Iberia during the opening of the North Atlantic. This evolution comprised four main rift phases: Late Triassic, Early Jurassic, Late Oxfordian and Early Cretaceous (e.g. Wilson et al. (1989); Kullberg (2000); Alves et al. (2003); Martinius and Gowland (2011); Kullberg et al. (2014)). The Lourinhã Formation, dated to the upper Kimmeridgian–lower Tithonian, was deposited during the "late post-rift" phase that followed the climax of the third rifting event. This stage is characterised by widespread continental to marginal–marine sedimentation in graben settings, with high subsidence rates and high sedimentation rates (Kullberg 2000; Alves et al. 2003; Kullberg et al. 2014). During the Late Jurassic, an intense extensional phase led to the development of

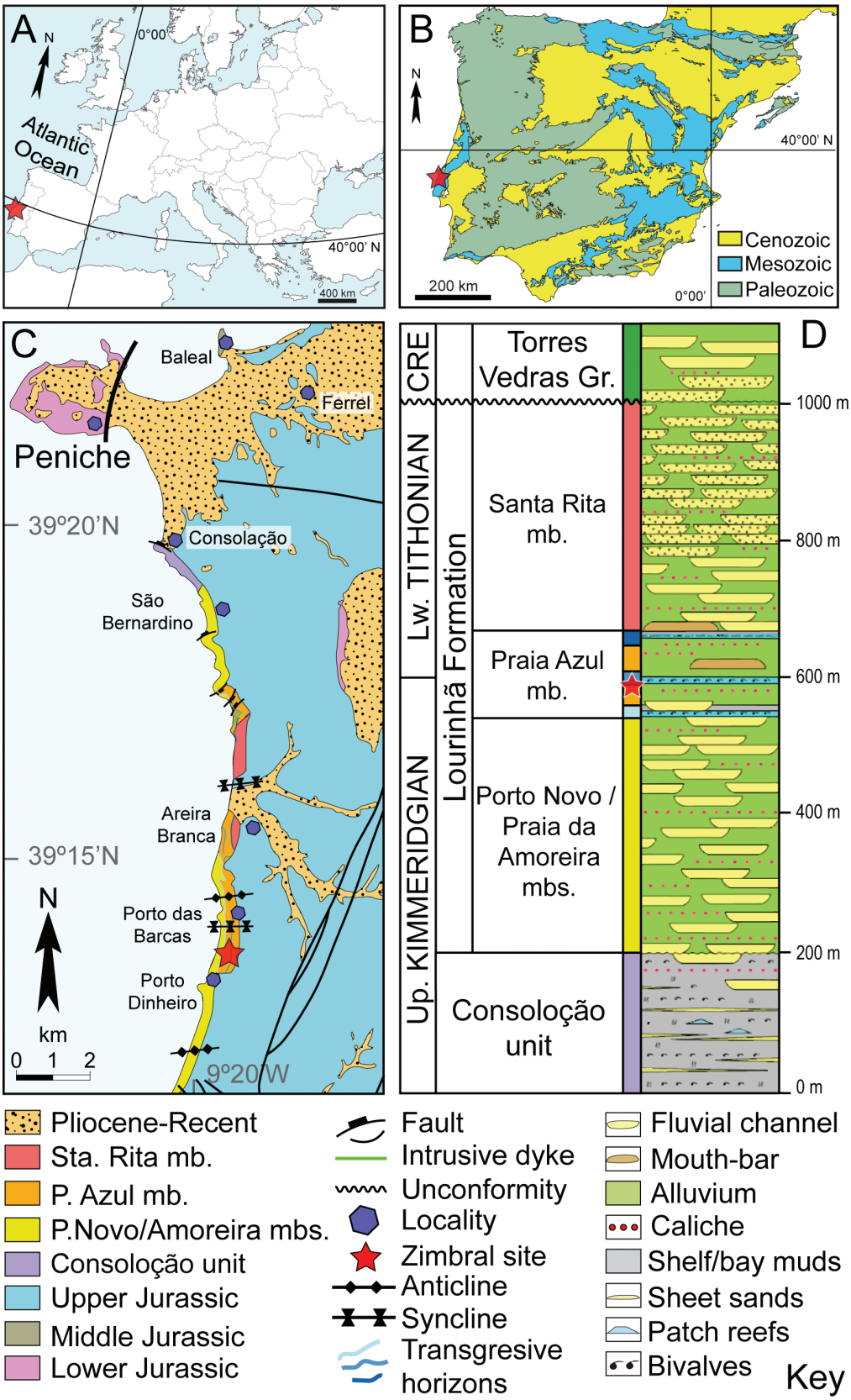

Figure 1. Geographical and geological location of the Zimbral VMA (site of ML2631 marked with red star). **A.** Europe map modified from Erin Dill; **B.** Simplified geological map of the Iberian Peninsula showing the location of the study area; **C.** Map of the onshore part of the Consolação Sub-basin and the lithostratigraphic units in the area south of Peniche, surroundings of Lourinhã, Portugal (modified from Taylor et al. (2014); Mateus et al. (2017)); **D.** Simplified lithostratigraphic framework of the Lourinhã Formation in the Consolação Sub-basin, showing key depositional elements (modified from Martinus and Gowland (2011); Taylor et al. (2014); Mateus et al. (2017)).

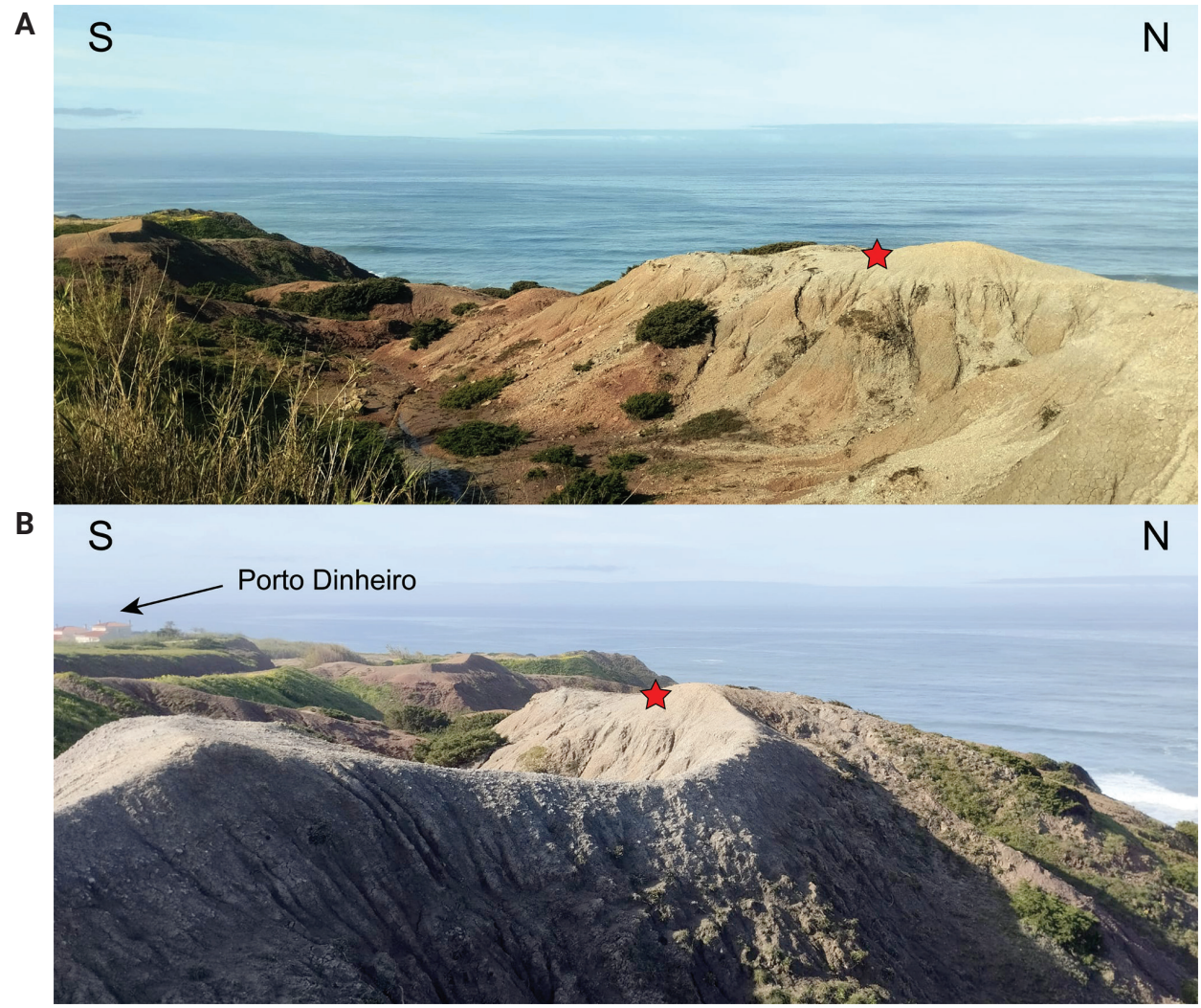

Figure 2. Photographs of the Zimbral VMA. **A, B.** Two different views of the Zimbral fossil site (near Porto Dinheiro, Lourinhã, Portugal) within the Praia Azul Member of the Lourinhã Formation (Kimmeridgian–Tithonian transition). The red star indicates the area where the nodule containing specimen ML2631 was discovered.

several sub-basins, including the Consolação, Bombarral–Alcobaça, Turcifal and Arruda Sub-basins, all bounded by active faults and influenced by salt tectonics (Leinfelder and Wilson 1998; Kullberg 2000; Alves et al. 2003; Taylor et al. 2014; Mateus et al. 2017). The study area of this work is located within the Consolação Sub-basin, which is bounded to the west by the Berlengas marginal basement horst system (Mateus et al. 2017). These tectonic features influenced subsidence rates and sediment supply, resulting in marked lateral facies changes and the accumulation of thick continental sequences dominated by fluvial and transitional environments.

The fossil ML2631 originates from the Zimbral vertebrate microfossil assemblage (Zimbral VMA) (Fig. 2), located in the lower part of the Praia Azul Member of the Lourinhã Formation, within the Consolação Sub-basin (Fig. 1C, D). The exact coordinates of the site are registered in the fossil locality catalogue of the Museu da Lourinhã (ML) and are available upon responsible request and decision of the Museum. The Lourinhã Formation spans the upper Kimmeridgian to lower Tithonian and comprises a complex alternation of fluvial (meandering), deltaic and marine-influenced facies. Specifically, the Praia Azul Member is characterised by heterolithic successions of mudstones and marls intercalated with shallow-marine carbonate beds, interpreted as the result of at least three regional transgressive episodes (Martinius and Gowland 2011; Taylor et al. 2014; Mateus et al. 2017). The fossil-bearing levels at Zimbral were deposited between the first and second of these transgressions and consist predominantly of grey marls and silty mudstones. These sediments are interpreted as representing low-energy floodplain or lagoonal environments, favourable for the preservation of small vertebrate remains (Guillaume et al. 2020).

Material and methods

The specimen ML2631 was collected by Micael Martinho and prepared by him at the vertebrate palaeontology laboratory of the Museu da Lourinhã (Portugal)

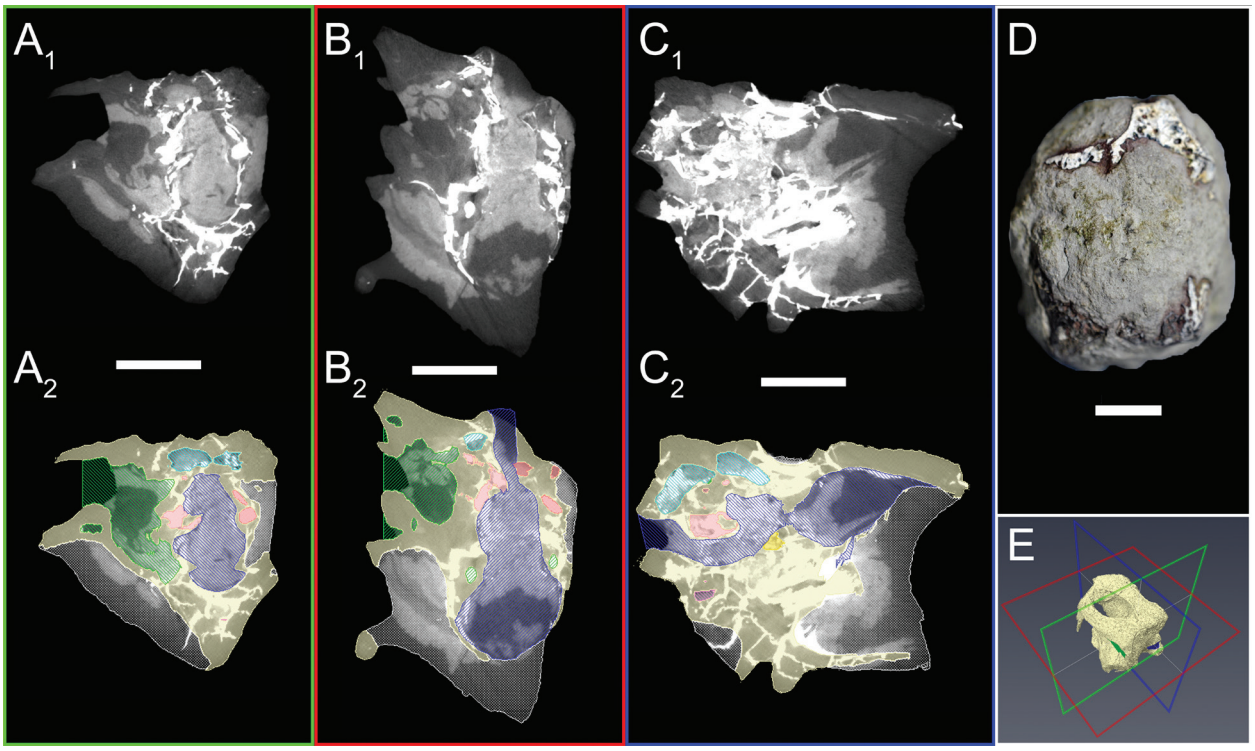

Figure 3. Micro-CT images of the specimen ML2631. **A_1, B_1, C_1.** Orthogonal CT slice views (XZ, XY and YZ planes, respectively) of ML2631 (see orientation in E); **A_2, B_2, C_2.** Segmentation examples illustrating the difficulty in identifying anatomical structures, with different elements marked for clarity: bone (yellow), matrix (white), brain cavity (blue), inner ear (light pink), pharyngotympanic cavity (green) and intertympanic diverticulum (sky blue); **D.** External appearance of the nodule of ML2631 prior to preparation, highlighting the areas where fossil bone was exposed at the surface. Scale bar: 1 cm.

under the supervision of the laboratory manager Carla Alexandra Tomás. The specimen was mostly prepared using a compressed-air micro-jack and precision hand tools due to the hardness of some mineralised portions of the nodule in which it was embedded. As a result, certain areas were left unprepared and still covered by matrix in order to preserve the integrity of the fossil.

To study these unexposed regions and the internal cavities of the skull, the specimen ML2631 was subjected to high-resolution micro-computed tomography (µCT) scanning at the Micronsense Metrologia Industrial Lda. facilities (Leiria, Portugal), with the micro-CT scanner GE VtomeX M 240 using a voltage of 200 kV and a current intensity of 500 µA. The resulting scan yielded 736 images with a voxel size of 0.049038 mm and an image resolution of 918 × 812 × 736 pixels. Raw data from the scan were imported, processed and segmented using AVIZO software 2020.3 (Thermo Fisher Scientific). The software was used on a workstation at the GeoBioTec Research Unit, Department of Earth Sciences, FCT, Universidade Nova de Lisboa, which holds an institutional licence. The 3D models obtained were rendered with BLENDER v. 3.5.0 (Blender Foundation). Access to the raw CT images is subject to the discretion of the institution housing the fossil, the Museu da Lourinhã (ML).

Although the specimen was micro-CT scanned, the presence of dense mineral veins (likely indicating the nodule is a septarian concretion) caused significant imaging artefacts, which obscured some regions of the skull and complicated segmentation (Fig. 3). Despite these limitations, it was possible to digitally reconstruct most of the skull, as well as several internal structures, including the brain cavity, inner ear and cranial nerve pathways (Fig. 5). All 3D models are available in Suppl. material S3. The models are also available in the digital repository MorphoSource (https://www.morphosource.org/) under Collection ID: 000768350 (https://www.morphosource.org/projects/000768350?locale=en).

The terminology and colour scheme used in Figs 4, 5 follow Witmer et al. (2008) for the brain cavities; Holliday and Witmer (2009) and Lessner and Holliday (2022) for the cranial nerves; and Dufeau and Witmer (2015) and Kuzmin et al. (2021) for the paratympanic sinus system and the inner ear. For ease of reading, the reconstructions of internal cavities that housed soft tissues and organs are, in some cases, referred to by the names of the soft tissues themselves (e.g. "brain" instead of "brain cavity endocast").

The phylogenetic analysis was performed under parsimony using TNT v.1.6 software (Goloboff and Morales 2023), based on the character matrix of Pochat-Cottilloux et al. (2024), which itself is derived from previous datasets by Turner (2015), Schwarz et al. (2017) and Venczel and Codrea (2019). With the addition of the new specimen ML2631, the matrix resulted in 81 taxa and 321 characters (Suppl. material 1). The analysis was conducted with a memory capacity of

1,000,000 trees, selecting *Gracilisuchus* as the outgroup taxon and using a New Technology Search that enabled all search algorithms (Sectorial Search, Ratchet, Drift and Tree Fusing; Goloboff (1999); Nixon (1999)). Following the analysis protocol of Pochat-Cottilloux et al. (2024), only the following default parameters were modified: 100 sectorial search drifting cycles, 100 ratchet iterations, 100 drift cycles, 100 rounds of tree fusing per replicate and using a driven search to find the minimum length 10 times. Characters were weighted equally and multistate characters were treated as unordered. To thoroughly explore tree space, this procedure was repeated using 10 different random starting seeds, selecting random seed = 0 (in TNT, the value 0 triggers a randomly generated seed). The trees resulting from each analysis were saved into a single .tre file. This procedure yielded 271 trees, which were subsequently filtered in TNT using the tree buffer filter to remove duplicates, resulting in 30 most parsimonious trees.

As an alternative to this phylogenetic analysis protocol, a single search was also performed with New Technology Search, with the same parameters, but using a driven search to find the minimum length 100 times (instead of 10), yielding the same results. To further validate the analysis and following the procedure of Pochat-Cottilloux et al. (2024), a heuristic search using Wagner trees with 1000 random addition sequences was conducted, followed by tree bisection–reconnection (TBR) and saving 10 trees per replication (random seed: 100). This search also yielded the exact same number of most parsimonious trees (30), tree length (1489 steps) and strict consensus topology.

Anatomical abbreviations: **A**, quadrate crest A; **aa.**, anterior ampula; **asc.**, anterior semicircular canal; **B**, quadrate crest B; **bo.**, basioccipital; **bot.**, basioccipital tuberosities; **br.**, brain cavity; **bs.**, basisphenoid; **bsd.**, basisphenoid diverticula; **bsr.**, basisphenoid rostrum; **car.**, cerebral carotid artery; **cc.**, common crus; **ch.**, choana; **chs.**, choanal septum; **cqp.**, cranioquadrate passage; **cer.**, cerebrum; **ECD**, Endosseous Cochlear Duct length; **eg.**, ear valve groove; **ex.**, exoccipital; **fc.**, foramen caroticum; **fh.**, hypoglossal foramen; **fm.**, formaen magnum; **fr.**, frontal; **frc.**, frontal crest; **fv.**, foramen vagi; **ie.**, inner ear; **its.**, intertympanic diverticula; **lbr.**, lateral bridge; **lg.**, lagena (cochlear duct); **ls.**, laterosphenoid; **lsc.**, lateral semicircular canal; **lss.**, laterosphenoid sinus; **mef.**, median eustachian foramen; **mps.**, medial pharyngeal sinus; **rps.**, rostral pneumatic sinus; **oa.**, otic aperture; **oc.**, occipital condyle; **ot.**, olfactory tract; **pa.**, parietal; **pac.**, parietal crest; **pas.**, parietal sinus; **pfo.**, pituitary (hypophyseal) fossa; **po.**, postorbital; **pob.**, postorbital bar; **pos.**, postorbital sulcus; **psc.**, posterior semicircular canal; **pt.**, pterygoid; **pts.**, pharyngotympanic sinus; **qu.**, quadrate; **si.**, siphoneal tube; **sif.** siphoneal foramen; **so.**, supraoccipital; **sq.**, squamosal; **stf.**, supratemporal fenestra; **stfo.**, supratemporal fossa; **V**, trigeminal foramen; $\mathbf{V_1}$, ophthalmic division of trigeminal nerve; $\mathbf{V_{2/3}}$, maxillomandibular ganglion of trigeminal nerve; $\mathbf{V_{so.}}$, supraorbital division of trigeminal nerve; $\mathbf{V_{pt.}}$, pterygoid division of trigeminal nerve; $\mathbf{V_{?}}$, unknown branch of trigeminal nerve; **ve.**, vestibule; **vls.**, ventral longitudinal sinus.

Institutional abbreviations: **ML**, Museu da Lourinã; **GEAL**, Grupo de Etnologia e Arqueologia da Lourinhã.

Systematic palaeontology

Crocodylomorpha Hay, 1930 (sensu Walker (1970))
Crocodyliformes Hay, 1930
Mesoeucrocodylia Whetstone & Whybrow, 1983 (sensu Benton and Clark (1988))
Neosuchia Benton & Clark, 1988
Atoposauridae Gervais, 1871
Atoposauridae indet.

Specimen ML2631

Anatomical description. ***General skull shape and ornamentation*****:** The dorsal surface of the preserved skull roof of ML2631 is heavily ornamented with pits and grooves; however, the remaining surfaces of the braincase and palate bones are mostly smooth. Although the right lateral margin is not preserved, the general shape of the skull roof can be inferred by applying the principle of symmetry. In dorsal view (Fig. 4A), it appears rectangular, with lateral margins that are approximately parallel. In dorsal view, the lateral bar formed by the squamosal and postorbital is approximately the same width as the interfenestral bar formed by the parietal and frontal although the latter is slightly wider. The supratemporal fenestrae are elliptical, with their major axis orientated anteroposteriorly (i.e. longer than wide). This elongate shape is accentuated by the presence of two distinct depressions or shallow fossae, located in the anterior and posterior regions of the fenestra (Fig. 4A). The posterior fossa is narrower, more acute and better defined, extending posteriorly between the squamosal–parietal suture. However, unlike other taxa, such as *Notosuchus terrestris* Woodward, 1896 (Fiorelli and Calvo 2008; Barrios et al. 2017) or the neosuchians *Wannchampsus kirpachi* Adams, 2014 and *Theriosuchus pusillus* Owen, 1879, this posterior depression or sulcus does not reach the posterior margin of the skull table. The anterior fossa is broader and situated along the anteromedial margin of the fenestra, extending over the frontal bone, in an arrangement similar to that observed in some eusuchians, such as Allodaposuchidae (e.g. Delfino et al. (2008); Puértolas et al. (2011); Puértolas-Pascual et al. (2014); Narváez et al. (2015)). The medial margin of the fenestra is bordered by a raised rim, whereas the lateral half is smooth and flat. None of the surrounding bones exhibit overhanging margins and the bones forming the fossa are visible in dorsal view, particularly in the posteromedial region, where the parietal, quadrate and laterosphenoid are clearly exposed due to the absence of a steep vertical wall in this area. Only the posteromedial margins of the orbits, formed by the frontal and postorbital, are preserved and no prominent

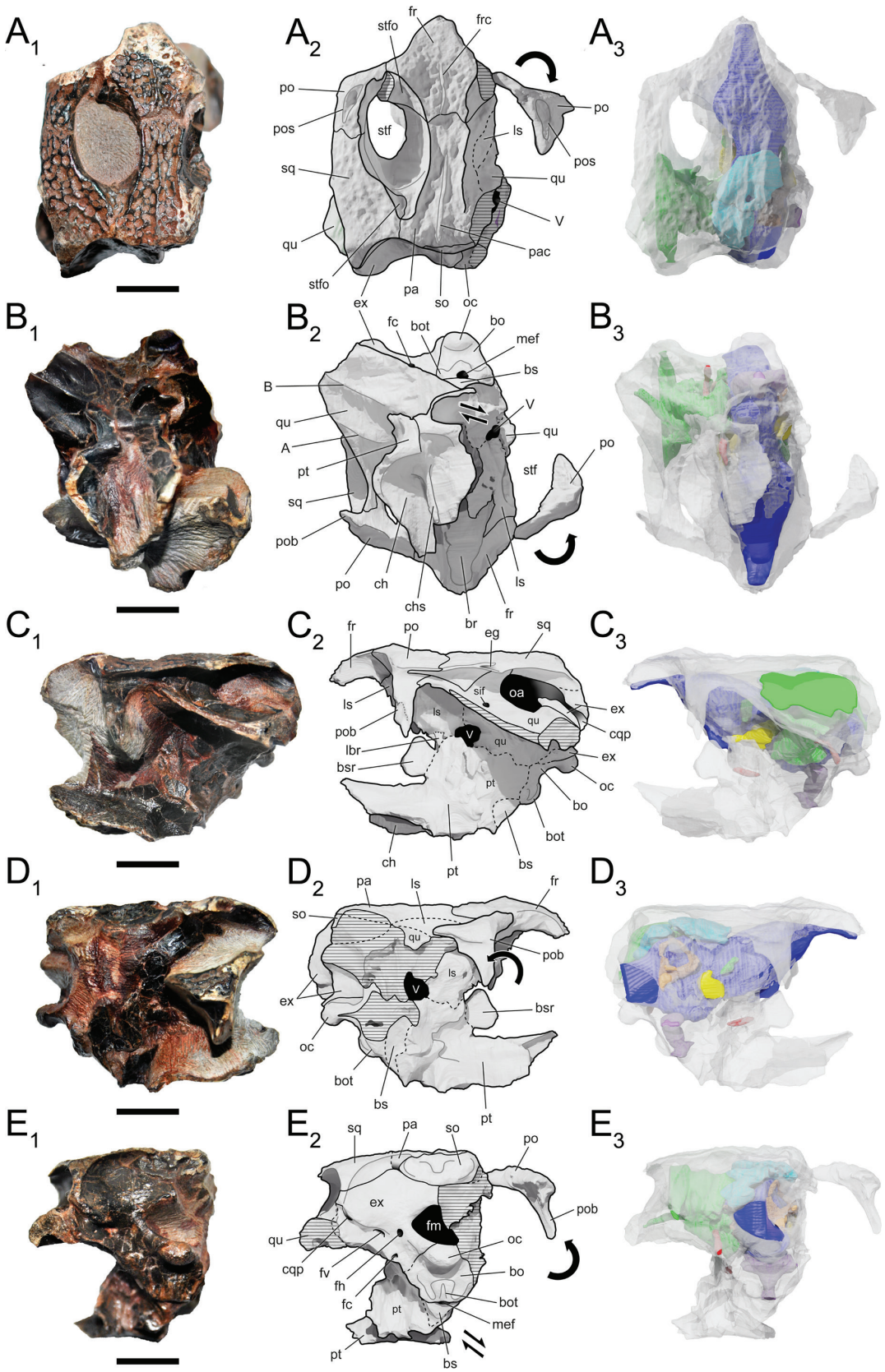

Figure 4. Photographs and illustrations of specimen ML2631. **A–E.** Different views of specimen ML2631: dorsal (**A**), ventral (**B**), left lateral (**C**), right lateral (**D**) and posterior (**E**). For each view, the fossil photograph (1), a 3D model with interpreted sutures and anatomical structures (2), and a semi-transparent 3D model showing the internal cavities (3) are shown. Hatched areas in A_2–E_2 indicate damaged or eroded regions, dashed lines mark uncertain sutures, curved bold arrows indicate the repositioning of the right postorbital bone to its original anatomical location, and parallel bold arrows indicate areas affected by shear deformation. See Material and methods section for anatomical abbreviations. Scale bar: 1 cm.

structures such as crests, depressions or raised rims are observed. Despite the limited orbital preservation, the gentle and open curvature of the postorbital and frontal margins suggests that the orbit was relatively large.

***Quadrate*:** A single, small subtympanic foramen (= siphoneal foramen) is present on the dorsal surface of the quadrate, located anterior to the otic aperture and situated within a shallow depression (Fig. 4C). In lateral view, the anterodorsal process of the quadrate clearly contacts the posteroventral region of the postorbital, just posterior to the ventral descent of the postorbital bar (Fig. 4C). Although the posterior articular region of the quadrate is not preserved, in lateral view, the major axis of the quadrate is directed posteroventrally. Ventrally, crest B of the quadrate is extremely sharp and well-defined in its lateral region, becoming progressively more curved, smoother and more robust as it extends ventromedially along the pterygoid ramus of the quadrate (Fig. 4B). As a result of this pronounced crest, the surface of the quadrate posterior to crest B is markedly concave, a condition also observed in other taxa such as *Leidyosuchus* (Wu et al. 2001), *Borealosuchus formidabilis* (Erickson, 1976) and *Protosuchus richardsoni* (Brown, 1933). Anteriorly and nearly parallel to crest B, a crest A of the quadrate can be observed, which is much shorter and less developed than the former (Fig. 4B).

***Quadratojugal*:** Although the quadratojugal itself is not preserved, the sutural surface with the quadrate is visible and allows the path of the bone to be inferred (Fig. 4C). Based on this, the dorsal process of the quadratojugal appears to be narrow and likely contacts only a small portion of the postorbital and may not contact it at all.

***Jugal*:** Although the jugal is not preserved, the facet for its contact with the postorbital is present on the postorbital bar and faces anteroventrally (Fig. 4C). As a result, the lateral surface of the postorbital bar would be formed by both the postorbital and the jugal. In addition, the postorbital process of the jugal, which forms the ventral half of the bar, should be directed posterodorsally or dorsally, but never anterodorsally.

***Frontal*:** In the specimen ML2631, the frontals are fused into a single, unpaired element, unlike the condition in basal crocodylomorphs and basal mesoeucrocodylians, in which the frontals are typically paired. The dorsal surfaces of both the frontal and parietal (Fig. 4A) are well ornamented with pits and bear a distinct midline ridge, although it is more subtle on the frontal, being restricted to its posterior half (Fig. $4A_2$). The presence of this sagittal ridge on the skull table is common in Atoposauridae, Paralligatoridae and some notosuchians (e.g. Turner (2015); Tennant et al. (2016)). The supratemporal roof formed by the frontal is dorsally flat, forming a well-developed skull table. This structure includes the postorbital and squamosal bones, which extend laterally as flat shelves projecting beyond the level of the quadrate contact. This condition contrasts with that of basal crocodylomorphs, such as sphenosuchians, in which the skull table is more complex, uneven and less laterally expanded (Spiekman et al. 2023). In dorsal view, the frontoparietal suture is positioned in the anterior portion of the interfenestral bar and is posteriorly concave (Fig. $4A_2$).

***Postorbital*:** Both postorbitals are preserved; however, the right postorbital was ventrally displaced from its original position (Fig. $4D_1$). Thanks to segmentation and 3D reconstruction, it was approximately restored to its original position (see curved arrows in Fig. 4). The dorsal surface of the postorbital is ornamented with pits and forms the anterolateral margin of the supratemporal fenestra and the posterolateral margin of the orbit (Fig. 4A). A large, elongate depression or sulcus, orientated anteromedially, is present on the dorsal surface of both postorbitals (Fig. $4A_2$). This feature has also been reported in other atoposaurids and paralligatorids (Tennant et al. 2016). The postorbital also forms the dorsal half of the postorbital bar, which is unsculpted, transversely flattened and dorsally constricted and clearly distinct from the dorsal surface of the postorbital (Fig. 4C). Although no vascular opening is evident along most of its dorsal surface, the CT scan reveals a large internal cavity within the bar and a small foramen seems to be present anteriorly, near the contact with the jugal portion of the postorbital bar. The postorbital lacks an anterolateral process, a feature that distinguishes it from most tethysuchians and some goniopholidids (e.g. Jouve et al. (2006); Salisbury and Naish (2011); Buscalioni et al. (2013)). Its dorsal portion on the skull table preserves the anterior and lateral edges, connected by a curved transition that gives the anterolateral margin a rounded appearance in dorsal view, forming an angle of approximately 115° between them (Fig. 4A). The bar separating the orbit from the supratemporal fossa is narrow, a condition that appears to result from a well-developed depression or fossa in the anteromedial region of the supratemporal fenestra, which reduces the anteroposterior width of the bar (Fig. 4A). This reduced bar is characteristic of most atoposaurids, except for *Knoetschkesuchus*, in which at least the larger specimens appear to have a broader bar (Schwarz et al. 2017). The lateral margins of the squamosal and postorbital, along the lateral bar of the supratemporal fenestra, are very thin dorsoventrally, forming a lamina in which the typical rims of the squamosal groove for the external ear valve musculature are not observed (Fig. 4C). This lamina extends horizontally in an anteroposterior direction, without any anterior flaring. In dorsal view, the contribution of the postorbital to the lateral bar of the supratemporal fossa is slightly less than that of the squamosal and the sinuous suture between these two bones lies approximately at the same anteroposterior level as the frontoparietal suture (Fig. $4A_2$).

***Parietal*:** In dorsal view, the parietal displays a flat, broad ornamented region separating the supratemporal fossae (Fig. 4A), in contrast to the very thin intertemporal bar or prominent crest observed in some taxa such as dyrosaurids (e.g. *Dyrosaurus*, *Sokotosuchus*; Jouve et al. (2006)) and sphenosuchians (e.g. *Terrestrisuchus*, *Dibothrosuchus*; Spiekman et al. (2023)). A subtle sagittal ridge extends from the posterior region along the

dorsal surface, reaching approximately two-thirds of the anteroposterior length of the bone (Fig. $4A_2$). Laterally, the parietal forms a well-defined, slightly elevated edge bordering the medial margin of the supratemporal fossae. The suture between the parietal and postorbital is not visible either on the dorsal surface of the skull roof or within the supratemporal fossa and is, therefore, probably absent. The occipital portion of the parietal is reduced and limited to a thin lamina visible above the supraoccipital (Fig. 4E). This lamina expands slightly laterally, projecting as a descending process that inserts between the supraoccipital (medially), the squamosal (laterally) and the dorsalmost tip of the exoccipital (ventrally) (Fig. $4E_2$).

***Supraoccipital*:** The supraoccipital is mainly visible in posterior (occipital) view, with only a very reduced contribution to the dorsal surface of the skull table, although it is still slightly dorsally exposed (Fig. $4A_2$). In posterior view, its outline is elliptical, being approximately 2.5 times as wide as it is tall (Fig. $4E_2$). It lacks the typical skull roof ornamentation of pits and grooves, but the posterior surface of the supraoccipital bears smooth bilateral prominences and a slightly more pronounced sagittal ridge, with two circular concavities located on either side (Fig. 4E). However, these features differ from the more pronounced prominences observed in other taxa, such as Dyrosauridae (Jouve et al. 2005; Jouve 2007). The supraoccipital is excluded from the foramen magnum, as the exoccipitals meet along the mid-line and form the lateral and dorsal margins of the foramen. Internally, an intertympanic sinus or recess (= intertympanic diverticulum in Dufeau and Witmer (2015); = transverse canal in Iordansky (1973); = mastoid antrum in Clark (1986)) can be observed in the CT images, extending through a transverse canal within the supraoccipital and below the parietal, establishing a connection between the middle ear regions (see Neuroanatomical description section, Fig. $5A_1$, D_1, E_1). In dorsal view, the supraoccipital contributes slightly to the skull roof, although this participation is minimal and restricted to the posterior-most margin of the cranial table (Fig. $4A_2$).

***Squamosal*:** Most of the dorsal surface of the squamosal is sculpted with pits, similar to the rest of the skull table (Fig. 4A). However, the posterolateral margin of the poorly-developed squamosal lobe (or prong) is smooth and apparently unornamented and seems to be aligned with the general level of the cranial table. In contrast, in many atoposaurids and paralligatorids, this prong presents a depression along the posterolateral margin that creates a step and a more ventrally positioned lobe relative to the skull table (e.g. Pol et al. (2009); Tennant et al. (2016)). However, this region was exposed to erosion while the skull was still encased in the nodule, so it cannot be ruled out that the step or the ornamentation was originally present, but was worn away. In dorsal view, a subtle lateral peak is observed along the lateral edge of the squamosal, approximately halfway along the bone (Fig. 4A, C). Only in this region, at the level of this peak, is there a lateral groove for the ear valve musculature (Fig. $4C_2$). Posterior to this point, the groove disappears and becomes a thin lamina without a middle sulcus, suggesting that the groove is discontinuous rather than straight and continuous. However, it remains unclear whether this peak is a genuine anatomical feature or an artefact resulting from the previously mentioned erosion. The presence of a discontinuous lateral groove has also been observed in some paralligatorids, such as *Paralligator* and *Shamosuchus* (Pol et al. 2009), as well as in some atoposaurids like *Aprosuchus ghirai* Venczel & Codrea, 2019 and certain specimens of *Varanosuchus wangleeorum* Pochat-Cottilloux, Lauprasert, Chanthasit, Manitkoon, Adrien, Lachambre, Amiot & Martin, 2024. In dorsal view, the squamosal is approximately twice as long anteroposteriorly as the postorbital. The posteromedial branch of the squamosal, which contacts the parietal, is transversely orientated and perpendicular to the sagittal axis. The posterior margin of this branch, between the squamosal prong and the parietal, is deeply concave in dorsal view, whereas, in posterior view, it appears straight. Due to matrix coverage and high-density artefacts in the CT images, the position, morphology and exposure of the opening of the temporo-orbital canal cannot be determined.

***Exoccipital* (≈ *Otoccipital*):** In Crocodylomorpha, the term "otoccipital" is commonly used to refer to the compound braincase element formed by the fusion of the exoccipital and opisthotic, as in other archosaurs (e.g. Iordansky (1973); Kuzmin et al. (2021)). In this study, for the sake of simplicity and following the most commonly used terminology in descriptive osteology, we will use the term "exoccipital".

The exoccipitals are mainly visible in posterior (occipital) view and their surface is smooth and lacks ornamentation. In this view, the two exoccipitals almost completely surround the foramen magnum, except for its ventral-most margin, which is formed by the basioccipital (Fig. 4E). The posterolateral region of the otic aperture, at the contact zone between the quadrate, squamosal and exoccipital bones, is partially obscured by dense matrix, hindering proper assessment of some sutures and structures in both the fossil and the CT images. However, the CT images rather suggest that these bones do not contact each other to form a fully closed cranioquadrate canal, which remains dorsolaterally open. In the contact area with the quadrate, the exoccipital appears slightly elevated dorsally, forming a crest that defines the lateral margin of the passage (Fig. $4C_2$). Consequently, the medial, ventral and most of the lateral margins of the passage seem to be formed exclusively by the exoccipital. This open cranioquadrate passage differs slightly from the condition observed in other clades, such as Allodaposuchidae, where it is less defined, more laterally open and developed within the exoccipital, being delimited ventrally by the exoccipital–quadrate suture and dorsally by the exoccipital–squamosal suture (e.g. Delfino et al. (2008); Puértolas et al. (2011); Puértolas-Pascual et al. (2014); Narváez et al. (2015)). The paroccipital processes extend laterally from the foramen magnum, but are reduced in size, as the portion projecting lateral to the cranioquadrate opening is very short (Fig. $4E_2$). Cranial nerves IX to XI exit the braincase through a single, large foramen vagi

situated ventral to the paroccipital process of the exoccipital, at the point where its ventral crest begins to develop and extend laterally (Fig. 4E). A foramen is also observed on the lateral rim of the foramen magnum, corresponding to the passage of cranial nerve XII and identified as the hypoglossal foramen. Below these foramina, the exoccipital tapers progressively until it contacts the basioccipital. Close to the tip of this wedge and adjacent to the lateral margin of the exoccipital, a foramen caroticum is visible for the passage of the carotid artery. This foramen is reduced in size, comparable to the vagus and hypoglossal foramina.

***Basioccipital*:** In lateral view (Fig. 4C, D), the basioccipital is inclined anteriorly and its posterior surface faces posteroventrally. This inclination, although less pronounced, is more comparable to the condition seen in most notosuchians, rather than in neosuchians, where the basioccipital tends to be vertically orientated (facing posteriorly) or even slightly posteriorly tilted (facing posterodorsally). In occipital view (Fig. 4E), the basioccipital shows a hexagonal outline. Its posterior surface bears prominent tuberosities positioned just below the occipital condyle. These tuberosities consist of a quadrangular mid-line projection bearing a sagittal crest, which extends ventrolaterally to connect with a pair of tuberosities positioned bilaterally on the basioccipital margins (Fig. $4E_2$). These lateral tuberosities ascend dorsally, although not enough to reach or contribute to the exoccipital. However, these tuberosities are not as pronounced as those observed in taxa, such as *Gavialis*, *Eothoracosaurus* or *Dyrosaurus*. Unfortunately, the arrangement of the lateral Eustachian tube openings (= pharyngotympanic canals in Dufeau and Witmer (2015) and Tucker (2017)) cannot be determined either in the fossil or in the CT images. On the contrary, the median Eustachian foramen (= median pharyngeal sinus in Witmer (1997), Nesbitt (2011) and Dufeau and Witmer (2015)) is large and well preserved (Fig. 4B).

***Basisphenoid*:** The anterior region of the basisphenoid is entirely covered by matrix; however, it could be segmented and interpreted thanks to the CT scan. The basisphenoid rostrum is not particularly elongated anteroposteriorly and exhibits a hatchet-like shape, being dorsoventrally narrower in its posterior region and reaching its maximum dorsoventral height anteriorly (Fig. 4C, D). In ventral view, the posterior portion of the ventral surface of the basisphenoid is anteroposteriorly shorter than that of the basioccipital (Fig. $4B_2$). Although the region is not well preserved — since the pterygoid has been displaced leftwards due to shear deformation (see arrows in Fig. $4B_2$), hindering the actual exposure of the basisphenoid — it appears that the basisphenoid was at least partially visible on the ventral surface of the braincase and not entirely excluded by the pterygoid and basioccipital. In lateral view, the basisphenoid is also exposed between the basioccipital and the pterygoids (Fig. $4C_2$, D_2). However, the exact limits of its sutures with the pterygoids, basioccipital and exoccipitals are difficult to discern.

***Laterosphenoid*:** Both laterosphenoids are preserved and exhibit a ventrolaterally swollen morphology, as they house a significant portion of the ventral region of a markedly inflated brain (see Neuroanatomical description section, Fig. 5). The left laterosphenoid is better preserved, allowing its boundaries and general morphology to be inferred. Unlike the condition observed in many adult neosuchian crocodylomorphs, such as Eusuchia, the laterosphenoid is relatively broad, being only about twice as long anteroposteriorly as it is wide mediolaterally. Anteriorly, the left laterosphenoid contacts and lies beneath the frontal, with a capitate process that appears to be orientated perpendicular to the sagittal axis. Interestingly, on the left laterosphenoid, the capitate process seems somewhat more oblique, as its anteromedial branch is orientated more anteroposteriorly (Fig. $4B_2$). This difference between the left and right laterosphenoids is most likely due to deformation; as a result, determining the true orientation of the capitate process in ML2631 is difficult. However, if the better preservation of the right laterosphenoid is to be trusted, it would suggest that the orientation of the capitate process is more mediolateral than anteroposterior. Posteriorly, the laterosphenoid contacts the pterygoid and quadrate and, dorsally, it contacts the parietal. At its junction with the pterygoid and quadrate, the laterosphenoid forms the anterior margin of the foramen vagi (Fig. $4C_2$, D_2). The presence of caudal and lateral bridges of the laterosphenoid is difficult to assess due to both the preservation of the fossil and the limited visibility of these structures in the CT scan images. However, the better-preserved left laterosphenoid appears to exhibit a lateral bridge for the passage of the ophthalmic division of the trigeminal nerve (V_1) (Fig. $4C_2$).

The distribution of laterosphenoid bridges for cranial nerves vary amongst crocodylomorphs (see Holliday and Witmer (2009) for a comprehensive overview of their distribution). In ML2631 and likely in other atoposaurids, at least a lateral bridge may already have been present (Fig. $4C_2$). However, whether this bridge was actually formed by the laterosphenoid or by the presence of an epipterygoid is difficult to determine from the available CT scan data. Although the ventral suture between the lateral bridge and the pterygoid seems to be visible, the dorsal end of the bridge is slightly detached from the laterosphenoid, seemingly due to taphonomic deformation. This separation could reflect a true sutural boundary, suggesting that the bridge may not be part of the laterosphenoid, but rather represents a very short epipterygoid.

Given the phylogenetic distribution of the laterosphenoid lateral bridge described in other taxa, this structure appears as a clearly derived feature within Eusuchia, particularly amongst Crocodylia. In contrast, more basal eusuchians and closely-related neosuchians either lack this structure or possess instead a well-developed epipterygoid. Therefore, in ML2631 (assigned to Atoposauridae, a clade recovered as deeply nested neosuchians or basal eusuchians in most phylogenetic analyses), the observed lateral bridge most likely corresponds to an epipterygoid rather than a laterosphenoid bridge. This interpretation is

consistent with the anatomical observations reported here and aligns well with the evolutionary transition proposed by Holliday and Witmer (2009).

***Pterygoid*:** The pterygoid wings of ML2631 are eroded and only the region surrounding the internal choana and the braincase wall is preserved. In addition, the sutural relationships between the pterygoid and adjacent bones, such as the quadrate, laterosphenoid, basisphenoid and basioccipital, are difficult to discern. On the lateral braincase wall, the pterygoid contacts the laterosphenoid and quadrate dorsally, forming the ventral border of the trigeminal foramen (Fig. $4C_2$, D_2). The preserved ventral surface of the pterygoids is entirely smooth, lacks ornamentation and the two pterygoids are fused posterior to the choana and anterior to the basisphenoid. Although the pterygoid flanges are broken, the small preserved portion reveals a horizontally orientated, laminar bone structure. The internal choanal opening enters the palate through a pronounced depression in the pterygoid (Fig. 4B), also known as the choanal groove. Although incomplete, the choana opens widely on to the ventral surface of the pterygoid, extending close to its posterior margin. Most of the choana is bordered by the pterygoids; however, the anterior portion of the palate, including the anterior margin of the choana, is missing. As a result, the total contribution of the pterygoids and palatines to the choana, as well as its position relative to the suborbital fenestrae, cannot be determined. The choanal opening is posteriorly closed by an elevated wall formed by the pterygoids. Laterally, these walls are more gently sloped, resulting in less defined lateral margins of the choana. The choanal opening appears to be elongated and is divided by a narrow vertical septum (Fig. 4B). However, due to preservation, it is difficult to determine whether the division of the choana by this septum is partial or complete.

Neuroanatomical description. Despite the presence of high-density mineralisations that generated artefacts in the CT images (as noted in previous sections and visible in Fig. 3), micro-computed tomography (μCT) scanning of ML2631 enabled the digital reconstruction of several internal cranial structures. Although these artefacts obscured portions of the neurocranium and made segmentation particularly challenging, careful analysis allowed for the interpretation and 3D reconstruction of a nearly complete brain endocast, parts of both left and right inner ears, several cranial nerves, a portion of the left internal carotid artery and most of the left paratympanic sinus system (Fig. 5).

***Brain*:** The brain cavity of ML2631 is nearly complete (blue colour in Fig. 5), although the olfactory bulbs and most of the olfactory tract are missing due to erosion of the anterior process of the frontal. Only the posterior portion of the olfactory tract is preserved, showing a gentle ventral curvature in lateral view and merging gradually with the cerebral hemispheres. In lateral view (Fig. $5C_2$, D_2), the brain exhibits the characteristic sigmoidal (S-shaped) profile typical of mesoeucrocodylians (Kley et al. 2010; Bona et al. 2013, 2017; Serrano Martínez et al. 2019b, 2021). This profile is defined by two inflection points: the cephalic flexure (CF), angle formed between the fore-brain and mid-brain and the pontine flexure (PF), between the mid-brain and hind-brain (e.g. Pierce et al. (2017); Erb and Turner (2021); Barrios et al. (2023)). This flexure ranges from straighter and more tubular brain endocasts, characterised by high CF and PF values, as seen in thalattosuchians, such as *Plagiophtalmosuchus* (CF = 175°; PF = 170°), *Macrospondylus* (CF = 170°; PF = 165°), *Steneosaurus* (CF = 170°–175°; PF = 165°–170°), *Cricosaurus* (CF = 166°; PF = 165°) and *Pelagosaurus* (CF = 160°; PF = 160°), to more flexed, sigmoidal brains with lower CF and PF values, as seen in crocodylians, such as *Alligator* (CF = 135°; PF = 145°), *Caiman* (CF = 138°; PF = 162°) (Pierce et al. 2017; Erb and Turner 2021) or *Trilophosuchus* (CF = 136°; PF = 142°) (Ristevski 2022). In ML2631, the estimated cephalic and pontine flexure angles are approximately CF = 150° and PF = 145°. These values fall within the typical range observed in other non-marine mesoeucrocodylians and contrast with the straighter endocasts of thalattosuchians, in which CF and PF values usually exceed 160° (Pierce et al. 2017; Erb and Turner 2021; Puértolas-Pascual et al. 2022, 2023).

The prosencephalon (or fore-brain) is bounded dorsally by the frontal and parietal bones, lateroventrally by the laterosphenoids and ventrally by the parabasisphenoid. In dorsal view, the cerebral hemispheres of the fore-brain appear rounded and laterally expanded (Fig. $5A_2$). The right hemisphere is notably smaller and posteriorly displaced, most likely due to taphonomic shear deformation also observed in other parts of the skull, such as the pterygoid. The left hemisphere is more spherical, better preserved and probably reflects the original morphology. In dorsal view, the contact between the olfactory tract and the expansion of the cerebral hemispheres is gradual. This contrasts with the more abrupt and rounded contact observed in taxa, such as crocodylians like *Alligator*, *Diplocynodon*, *Osteolaemus* or *Trilophosuchus*; in dyrosaurids like *Rhabdognathus*; or in thalattosuchians, such as *Macrospondylus* (Serrano-Martínez 2019; Erb and Turner 2021; Ristevski 2022; Barrios et al. 2023). This transition, therefore, would be more gradual and comparable to that observed in taxa, such as *Alligator*, *Diplocynodon* and *Osteolaemus*, but not as gradual as in taxa, like *Gavialis*, *Thoracosaurus*, *Portugalosuchus* or *Pholidosaurus*, which exhibit a more triangular than rounded dorsal outline transition of the olfactory tract and cerebral hemispheres (Serrano-Martínez 2019; Barrios et al. 2023; Puértolas-Pascual et al. 2023). The pituitary or hypophyseal fossa, located ventral to the fore-brain region (Fig. $5C_2$, D_2), is poorly preserved. The surrounding bones of the fossa are fragmentary and damaged and as such, this area was reconstructed tentatively based on limited preserved structures and CT data. If the reconstruction and interpretation are correct, the pituitary appears to project posteriorly in an almost subhorizontal orientation, a condition also observed in some thalattosuchians (Ristevski 2022; Puértolas-Pascual et al. 2023).

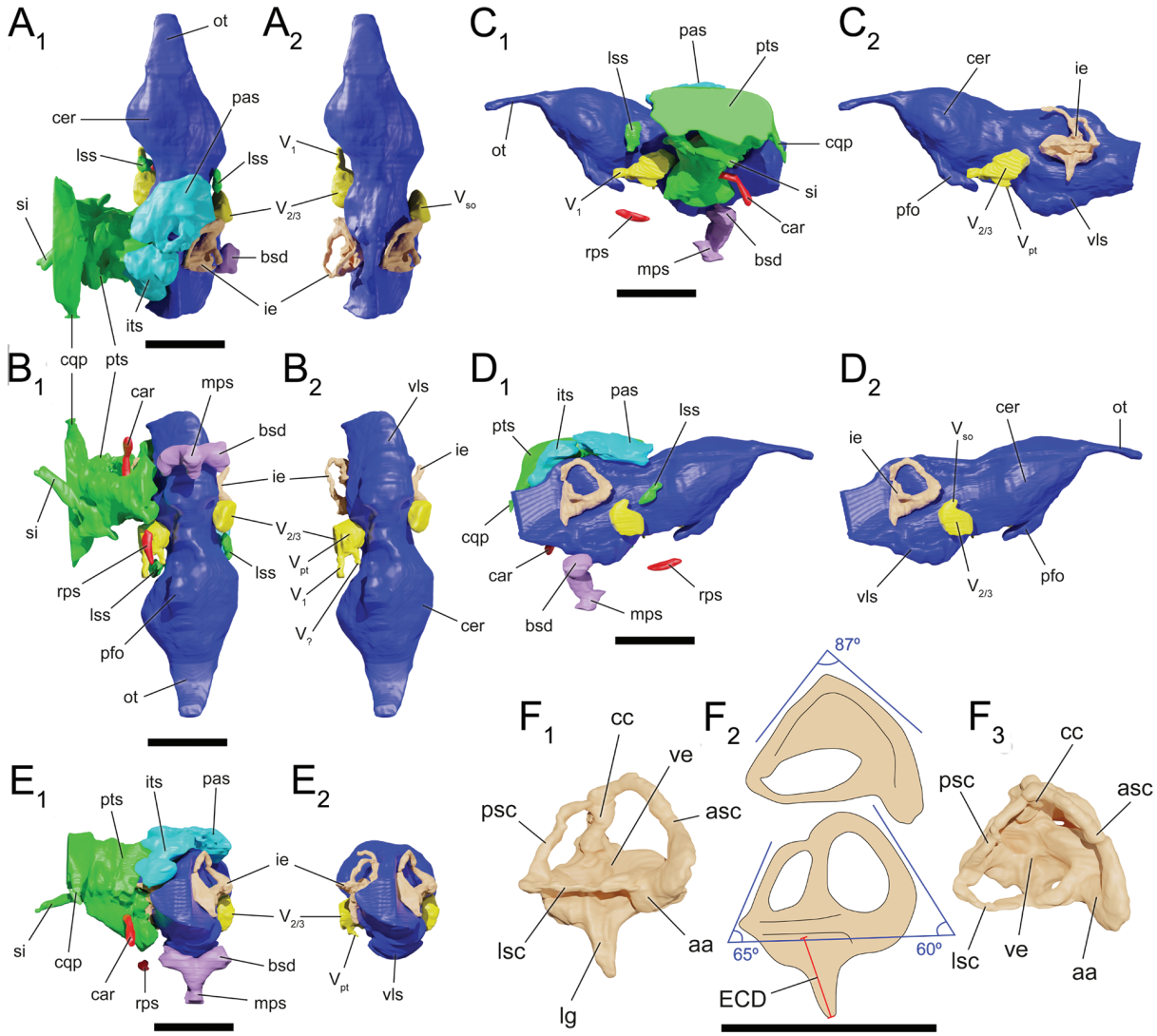

Figure 5. 3D reconstruction of the cranial cavities of the braincase of ML2631. **A.** Dorsal; **B.** Ventral; **C.** Left lateral; **D.** Right lateral; **E.** Posterior views; **F.** 3D reconstruction of the right inner ear, completed using mirrored elements from the left one, shown in lateral (F_1) and dorsal (F_3) views, along with a schematic reconstruction (F_2) to illustrate measurements and angular relationships. Cavity colours: brain cavity (blue), inner ear (light pink), pharyngotympanic sinus (green), intertympanic diverticulum (sky blue), parietal sinus (sky blue), median pharyngeal sinus (purple), carotid artery (red) and cranial nerves (yellow). See Materials and methods section for anatomical abbreviations. Scale bar: 1 cm.

In lateral view, the dorsal transition between the prosencephalon and the mesencephalon (mid-brain) is subtle and is characterised by a narrowing with both lateral and dorsal concavities between the cerebral hemispheres and the region of the optic lobe (Fig. $5C_2$, D_2). This constriction is more clearly visible in dorsal view, where it marks the position of the optic lobe (Fig. $5A_2$). Posterior to this 'neck' region, the mesencephalon contacts the rhombencephalon (hind-brain), which expands dorsoventrally until reaching the maximum thickness of the brain. The boundary between the mesencephalon and the rhombencephalon (hind-brain) is defined by the posterior margin of the trigeminal nerve (cranial nerve V) opening and the anterior edge of the concavities that accommodate the otic capsules.

In lateral view, the rhombencephalon is strongly developed dorsoventrally and defined by convexities on both the dorsal (cerebellum) and ventral (ventral longitudinal sinus) surfaces (Fig. $5C_2$, D_2). Dorsally, this region shows pronounced constrictions on both sides, resulting in broad lateral depressions that enclose the otic capsules and inner ear (Fig. $5A_2$, E_2). Coinciding with the area of maximum ventral expansion of the rhombencephalon, the region of the ventral longitudinal sinus exhibits a lateral constriction that creates an anteroposterior groove on each side of the brain (Fig. $5C_2$, D_2, E_2). However, this constriction appears to be an artefact caused by the medial displacement of the ventral process of the prootic at its contact with the basisphenoid. In lateral view, the posterior region of the hind-brain narrows dorsoventrally, gradually decreasing in thickness towards the medulla. Only the left half of the medulla is preserved; the right side appears to be lost due to erosion. The medullary region is elliptical in cross-section, being approximately twice as wide lateromedially as it is high dorsoventrally (Fig. 5C). In addition, the rhombencephalon of ML2631 is proportionally longer than in most other compared crocodylomorphs. It represents

about 55–60% of the total brain length (from the anterior region of the cerebral hemispheres to the posterior end of the medulla), showing a proportion similar to that of *Rhabdognathus* (Erb and Turner 2021). In the other taxa, however, it usually accounts for less than 50% (around 45%). This relatively greater length cannot be attributed to an earlier ontogenetic stage and, instead, supports the interpretation of ML2631 as an adult individual, since the rhombencephalon is known to increase proportionally during brain development (see 3D models in Jirak and Janacek (2017), Hu et al. (2020), and Barrios et al. (2023)).

***Cranial nerves*:** Only the left and right trigeminal nerves (cranial nerve V) of ML2631 are preserved or visible in the CT scan (yellow colour in Fig. 5). As in other archosaurs, the trigeminal nerve is the largest cranial nerve, with both motor and sensory functions. It branches into three main divisions: ophthalmic (V_1), maxillary (V_2) and mandibular (V_3), along with several secondary branches, such as the supraorbital rami (V_{so}) (e.g. Lessner and Holliday (2022)). In ML2631, some of these branches are partially preserved. The trigeminal nerve (V) emerges laterally from the mesencephalon and exits the braincase through a large, subcircular foramen bordered by the prootic, laterosphenoid, quadrate and pterygoid. The right trigeminal nerve is positioned more posteriorly than the left (Fig. $5A_2$), a condition that may result from shear-related deformation, which, as previously mentioned, also appears to have affected the right cerebral hemisphere. The left trigeminal nerve is better preserved, showing the ophthalmic branch (V_1), the maxillomandibular ganglion ($V_{2/3}$) — from which the maxillary (V_2) and mandibular (V_3) divisions originate — and the secondary pterygoid branch (V_{pt}) (Fig. $5A_2$, C_2, B_2). On the right side, only the maxillomandibular ganglion ($V_{2/3}$) and the supraorbital ramus (V_{so}) could be partially reconstructed (Fig. $5D_2$).

The ophthalmic division (V_1) is partially preserved on the left side, projecting anteriorly from the main trigeminal ganglion ($V_{2/3}$) and passing through the lateral bridge of the laterosphenoid/epipterygoid (Figs $4C_2$, C_3, 5). There appears to be an additional branch ($V_?$) that follows a trajectory similar and nearly parallel to V_1, although it is positioned more medially (Fig. $5B_2$). However, this division has not been reported in other crocodylomorphs with well-known cranial nerve anatomy, such as *Alligator* (Lessner and Holliday 2022), so it remains uncertain whether this structure is genuine or an artefact caused by preservation. The maxillary (V_2) and mandibular (V_3) branches would have projected anteriorly and lateroventrally, respectively, from the trigeminal ganglion ($V_{2/3}$) and foramen. However, since they do not contact the surrounding bones along their course, they typically leave little to no trace on the braincase wall. Thanks to the CT scan, a small branch was also segmented in the ventral region of the $V_{2/3}$ ganglion, projecting ventromedially (Fig. $5C_2$, B_2, E_2). This branch may correspond to the pterygoid division (V_{pt}) of the trigeminal nerve (Lessner and Holliday 2022). The preservation of the right trigeminal nerve is limited, with only the main $V_{2/3}$ ganglion visible, along with a small dorsal projection that may correspond to the supraorbital branch (V_{so}) of cranial nerve V (Fig. $5A_2$, D_2). Due to preservation limitations, it is not possible to determine whether this V_{so} branch passes through a caudal bridge of the laterosphenoid.

***Paratympanic sinus system*:** The paratympanic system comprises a series of pneumatic cavities primarily located around the inner ear and adjacent regions of the neurocranium. In ML2631, the left pharyngotympanic sinus system, left intertympanic diverticula, parietal sinus and median pharyngeal sinus system are preserved. These pneumatic structures are housed within bony recesses mainly surrounding the hind-brain and part of the mid-brain (Fig. 5).

The pharyngotympanic sinus (green color in Fig. 5) is the largest and most complex cavity of the paratympanic sinus system, extending laterally from the inner ear region towards the external auditory meatus (Fig. 5A–C). As it approaches the external auditory meatus, the pharyngotympanic sinus shows a marked anteroposterior expansion, more developed posteriorly. This posterior expansion corresponds with the cranioquadrate passage, which, in ML2631, is delimited exclusively by the exoccipital and remains dorsolaterally open. Additionally, in the ventromedial region, the pharyngotympanic sinus surrounds the internal carotid artery and extends ventrally beneath the brain. The lateral pharyngotympanic tubes, which connect to the pharynx and open externally through the lateral pharyngotympanic (Eustachian) foramina, are not preserved. Ventral to the external auditory meatus, the left siphonial tube is preserved. This structure runs posterolaterally through the quadrate and would have exited via the foramen aereum, although this foramen is not preserved due to erosion of the posterior end of the quadrate. In each laterosphenoid, a dorsoventrally orientated cavity is preserved in the central region of the bone. These laterosphenoid sinuses appear to be isolated and do not connect to any of the larger adjacent cavities (Fig. 5A, B).

The origin and functional significance of the median pharyngeal sinus in Crocodylomorpha remain poorly understood and its orientation appears to vary ontogenetically, becoming more vertical in larger individuals, in parallel with the progressive verticalisation of the basioccipital (Witmer and Ridgely 2009; Dufeau and Witmer 2015; Serrano-Martínez et al. 2019a). The median pharyngeal sinus of ML2631 (purple colour in Fig. 5), located along the sagittal plane, forms a robust canal that projects anteroventrally until it expands and opens externally through the median pharyngeal foramen between the basioccipital and the basisphenoid. This canal is relatively short and robust when compared to the condition observed in crocodylians and other eusuchians, such as allodaposuchids, in which the canals are notably more slender, elongated and directed ventrally or posteroventrally (e.g. Serrano-Martínez (2019); Serrano-Martínez et al. (2019a, 2019b); Puértolas-Pascual et al. (2022, 2023)). The cross-section of the canal is not perfectly circular along its trajectory, as it is slightly anteroposteriorly oval, with a more flattened anterior margin that becomes progressively broader than the posterior one towards the

external opening, resulting in a drop-like shape. This contrasts with the condition observed in crocodylians: in alligatoroids, the cross-section is circular, whereas, in crocodyloids, it is D-shaped, with the flat side facing anteriorly (Serrano-Martínez et al. 2019b). Dorsally, this sinus bifurcates into a Y-shaped configuration that connects dorsally to the basisphenoid diverticula (Fig. 5E$_1$). The connection between these diverticula and the pharyngotympanic sinuses could not be segmented due to poor visibility of this region in the CT images.

The preserved left intertympanic diverticulum (sky blue colour in Fig. 5) is positioned dorsally to the brain, pharyngotympanic sinuses and inner ear and it is housed within the supraoccipital, exoccipital and prootic. This complex consists of a lateral cavity that extends approximately twice as far posteroventrally as it does laterally (Fig. 5A$_1$, D$_1$, E$_1$). This reduced lateral extension of the intertympanic diverticulum is similar to that observed in taxa such as *Alligator*, *Caiman* and *Osteolaemus* and contrasts with other eusuchians, such as *Portugalosuchus*, *Gavialis*, *Tomistoma* and *Crocodylus*, in which the lateral expansion is much more developed (Serrano-Martínez 2019; Puértolas-Pascual et al. 2023). Perrichon et al. (2023) demonstrated that, in extant crocodylians, the intertympanic sinus undergoes significant ontogenetic changes: during growth, its shape becomes more laterally elongated and compressed anteroposteriorly and dorsoventrally. Nevertheless, it correlates closely with overall cranial morphology, allowing discrimination between lineages (e.g. Alligatoridae vs. Longirostres, Crocodylidae vs. Gavialidae). Though the ontogenetic stage of ML2631 is uncertain, its size falls within the adult range for an atoposaurid and its cranial proportions, well-marked ornamentation and advanced degree of neurocranial fusion do not support a very early developmental stage (Schwarz et al. 2017). Its greater dorsoventral development compared to the lateral expansion may, therefore, reflect either a moderately young ontogenetic stage or a clade-specific morphological pattern. Unfortunately, further investigation, based on µCT-derived ontogenetic series and additional specimens, will be required to test these alternatives.

ML2631 preserves a sagittally placed parietal sinus (sky blue colour in Fig. 5) that extends into the parietal bone, anterior to the intertympanic diverticula. This sinus extends anterodorsally over the cerebral cavity and reaches the anterior region of the mid-brain. Its posterior margin is ring-shaped and clearly visible in dorsal view (Fig. 5A$_1$). This ring-shaped morphology, formed by the anterolateral pre-parietal processes and the intertympanic pneumatic recess, has also been observed in other taxa such as *Crocodylus*, *Melanosuchus*, *Caiman* and *Osteolaemus* (Serrano-Martínez 2019; Perrichon et al. 2023).

***Inner ear*:** In ML2631, both inner ears (light pink colour in Fig. 5) are partially preserved. These structures are housed within the dorsolateral otic capsules of the rhombencephalon, which are formed by the prootics and exoccipitals. The inner ear comprises the bony labyrinth, a complex system of interconnected semicircular canals and cavities. This system encloses the vestibule and other neurosensory organs responsible for balance, as well as the cochlear region involved in hearing. Neither of the inner ears is completely preserved; however, the left one is nearly complete (Fig. 5C$_2$), while the right one preserves only the anterior half (Fig. 5D$_2$). By mirroring and digitally superimposing both models, a tentative reconstruction of the complete inner ear morphology can be generated (Fig. 5D).

The anterior semicircular canal is the longest, thickest and most dorsally extended of the three canals. In lateral view (Fig. 5D$_2$, F$_1$, F$_2$), it rises anterodorsally from a long, vertical and slender crus commune until reaching the highest point of the inner ear. The cross-sectional diameter of the crus commune is comparable to that of the anterior canal itself. From the top, the anterior canal descends gradually in an anteroventral direction to connect with the vestibule and the lateral (horizontal) semicircular canal. The junction between these structures, known as the anterior ampulla, projects anteriorly from the main body of the inner ear. The posterior semicircular canal exhibits a morphology similar to that of the anterior canal, but orientated in the opposite direction and slightly smaller in size. It originates posteriorly from the crus commune and descends posteroventrally until it connects with the lateral semicircular canal in the posterior region of the inner ear. At the junction, the posterior ampulla forms a slight projection, less pronounced than that of the anterior ampulla. The overall diameter of the ring formed by the posterior canal is smaller and the cross-sectional diameter of its duct is also slightly reduced compared to that of the anterior canal. In dorsal view (Fig. 5F$_3$), the angle between the planes of the anterior and posterior semicircular canals measures approximately 87°. The lateral semicircular canal is positioned lateral to the vestibule and forms a ring that lies approximately in the horizontal plane. It is similar in length and cross-sectional diameter to the posterior canal and its ring diameter is also comparable, although slightly larger. In lateral view, the angle formed by the lateral and the anterior canals is about 60° and the angle between the lateral and the posterior canals is about 65° (Fig. 5F$_2$). The cochlear ducts (lagena) of both inner ears are ventrally projected, although their morphology and full ventral extent are difficult to determine due to preservation.

The endosseous labyrinth of ML2631 exhibits an intermediate morphology between that of terrestrial and semi-aquatic crocodylomorphs. The markedly elevated anterior semicircular canal, combined with a tall and slender crus commune, resembles the condition described for fully terrestrial taxa (e.g. *Protosuchus*, *Junggarsuchus*, *Simosuchus* and *Baurusuchus*) (Kley et al. 2010; Schwab et al. 2020; Dumont et al. 2022; Barrios et al. 2023). However, the moderately thick canal cross sections and the overall proportions of the labyrinth, which is not dorsoventrally compressed, are more similar to those of eusuchians and extant crocodylians than to the slightly flatter labyrinths of teleosauroids (e.g. *Steneosaurus*,

Macrospondylus) or the compact semicircular canals with broad cross-sectional diameters typical of pelagic metriorhynchids (e.g. *Cricosaurus*, *Torvoneustes*) (Schwab et al. 2020; Wilberg et al. 2022). This similarity is further supported by the marked asymmetry between the anterior and posterior semicircular canals, which mirrors the condition seen in some eusuchians and crocodylians and contrasts with the more symmetrical canal arrangement observed in teleosauroids and metriorhynchids (Serrano 2019; Schwab et al. 2020; Barrios et al. 2023). Taken together, these features suggest that ML2631 retained a vestibular system well-suited for balance control and equilibrium in a primarily terrestrial context, as inferred from the association between tall, elongate semicircular canals and increased angular sensitivity in terrestrial vertebrates (Spoor et al. 2002; Schwab et al. 2020), while the moderately thick canals and non-compressed labyrinth proportions support a functional interpretation compatible with a moderately amphibious or nearshore lifestyle.

Neurosensorial capabilities. The neurosensory capabilities of ML2631 have been partially estimated following the methodology proposed by Serrano-Martínez (2019) and further developed in Serrano-Martínez et al. (2019b, 2021, 2025). Unfortunately, some of these estimates could not be reliably calculated. In particular, olfactory capacity could not be estimated, as it requires the dimensions of the olfactory bulbs, which are not preserved in the specimen. Likewise, the Reptile Encephalisation Quotient (REQ; Hurlburt (1999)), which is designed to estimate cognitive capabilities in reptiles, based on endocast volume relative to body mass, was not calculated due to the fragmentary nature of the specimen. Most available equations for body mass estimation (e.g. Dodson (1975); Webb and Messel (1978); Platt et al. (2011)) rely on cranial measurements that are either absent or poorly preserved in ML2631. Moreover, these equations are primarily based on extant crocodylians, which may have different skull-to-body proportions compared to atoposaurids. Nevertheless, by comparing and rescaling the size of the skull table with reference to more complete atoposaurid skeletons and other neosuchians, we estimate that ML2631 had a total body length between 0.5 and 1 metre, probably closer to 0.8 metres. However, such a rough approximation prevents us from calculating the REQ with confidence.

However, auditory capacity was estimated, based on the length of the endosseous cochlear duct (ECD) of the inner ear (Fig. 5F$_2$), following the methodology outlined in Serrano-Martínez (2019) and based on the equations of Walsh et al. (2009). The ECD length was estimated at 4.01 mm and the basicranial length (from the caudalmost point of the basioccipital condyle to the medialmost point of the pterygoid–palatine suture) at 40.13 mm. These approximate values yield a ratio of 4.01/40.13 = 0.099, with a logarithmic transformation of log0.099 = −1. Due to the poor preservation of the cochlear region and the absence of the pterygoid–palatine suture, both measurements should be considered approximate. This value of −1 falls within the range observed in other eusuchians, such as Allodaposuchidae and Crocodylia (−0.73 to −1.09) (Serrano-Martínez 2019) and it is also close to the values reported by Walsh et al. (2009) (−0.62 to −1). These results suggest an auditory adaptation to low-frequency sounds, a condition also observed in other eusuchians and, as demonstrated by this specimen, likely already present in atoposaurids. Low-frequency hearing is typically associated with the ability to detect environmental signals, such as water movement, distant vocalisations or low-pitched intraspecific communication. In modern crocodylians, such sensitivity may facilitate social behaviour, the detection of predators or prey or mate localisation in turbid or enclosed environments (Garrick and Lang 1977; Brown and Waser 1984; Walsh et al. 2009).

Visual acuity could be estimated thanks to the relatively good preservation of the brain cavity in ML2631. For this analysis, the volume of the mesencephalon, which houses the optic lobe, was compared to the total brain volume. In crocodylians, the optic lobe is easily identifiable within the mesencephalon and its relative volume has been used as a proxy for visual capability (Jirak and Janacek 2017; Serrano-Martínez 2019). ML2631 has an approximate total brain volume of 1716.02 mm³ and a mesencephalic volume of 154.2 mm³, resulting in a ratio of 0.0898 or 8.98%. In extant crocodylians, the relative volume of the mesencephalon ranges from 10% to 15% in large-sized individuals and from 19% to 22% in medium-sized ones (Serrano-Martínez 2019). The mesencephalic ratio of 8.98% in ML2631 is closer to the lower end of the range observed in large-bodied living species, suggesting a comparable level of visual acuity. This is particularly notable given the very small estimated total body length of ML2631, just under 1 m. In extant crocodylians, smaller individuals tend to have a proportionally larger mesencephalon and optic lobe, which is thought to reflect improved visual capacity. The small mesencephalon of ML2631, despite its diminutive body size, deviates from this general trend and more closely resembles the condition seen in large, mature individuals. This pattern may support the hypothesis that ML2631 was a fully grown individual exhibiting the dwarf adult body size characteristic of atoposaurids, with visual capabilities consistent with its neurological maturity rather than its reduced body size.

Phylogenetic analysis

All cladistic analyses performed (see Material and methods section for analytical protocol) recovered a total of 30 most parsimonious trees, each with a tree length of 1489 steps. The analysis yielded a consistency index (CI) of 0.260, a retention index (RI) of 0.592 and a rescaled consistency index (RC) of 0.154. The strict consensus tree is shown in Fig. 6. It focuses on Neosuchia and more basal clades not related to ML2631, such as Sphenosuchia, Protosuchia and Notosuchia, have been omitted to save space and improve figure clarity. The complete strict consensus tree,

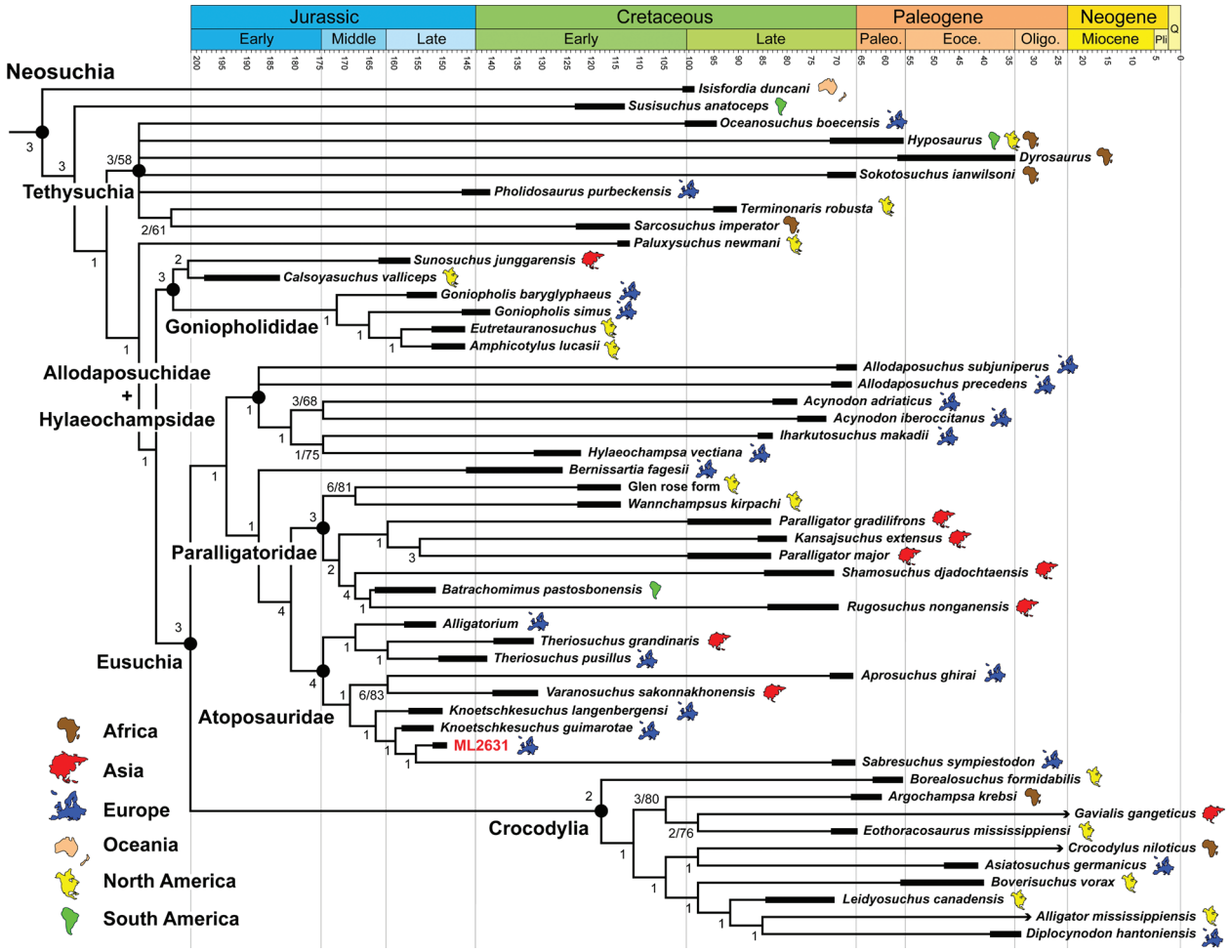

Figure 6. Phylogenetic relationships of Neosuchia, showing the position of ML2631 (in red). Analysis based on the matrix of Pochat-Cottilloux et al. (2024). Time-calibrated strict consensus tree of 30 most parsimonious cladograms (tree length = 1489 steps). Numbers at nodes indicate Bremer support values above 1 and bootstrap frequencies above 50%. Extant species are indicated by terminal branches ending in arrows.

including all clades and the 81 taxa, is available in the Suppl. material 2. Bootstrap frequencies above 50% and Bremer support values greater than 1 for each node are indicated in the strict consensus tree (Fig. 6).

The overall topology of the consensus tree (Fig. 6) is almost identical to that obtained by Pochat-Cottilloux et al. (2024), although the addition of ML2631 has resulted in a significant improvement in the resolution of Atoposauridae. As in their analysis, *Isisfordia* and *Susisuchus* occupy the basalmost positions within Neosuchia (Turner and Pritchard 2015; Venczel and Codrea 2019), followed by a series of successive monophyletic sister clades, including Tethysuchia, Goniopholididae and Eusuchia, all moderately well supported with Bremer support values of 3.

Interestingly and as previously recovered in other phylogenetic analyses, the clades Paralligatoridae, Atoposauridae and Bernissartiidae (traditionally considered advanced non-eusuchian neosuchians) appear here nested within Eusuchia (Turner 2015; Schwarz et al. 2017; Venczel and Codrea 2019; Pochat-Cottilloux et al. 2024). This result mirrors the topology retrieved by Pochat-Cottilloux et al. (2024), who also recovered a monophyletic Eusuchia including these groups along with Hylaeochampsidae, Allodaposuchidae and Crocodylia. In my analysis, the definition of Eusuchia relied on a set of common unambiguous synapomorphies, including undivided choanal grooves, cervical and trunk procoelous vertebrae, more than two rows of dorsal osteoderms with a discrete convexity on the anterior margin and an exposed supraoccipital in the skull roof. These characters are nearly identical to those obtained by Pochat-Cottilloux et al. (2024), except that their analysis did not recover procoelous trunk vertebrae (character 93) as an unambiguous synapomorphy, but only in the cervicals. However, they noted that these features are homoplastic and potentially influenced by ontogenetic or preservational factors (see also Salisbury et al. (2006); Turner and Pritchard (2015); Leite and Fortier (2018); Martin et al. (2020)). Notably, the presence of fully pterygoid-bound choanae, historically regarded as a diagnostic eusuchian trait, is now recognised as having evolved independently in several lineages including *Varanosuchus*, Hylaeochampsidae, Allodaposuchidae and Crocodylia

and, thus, cannot be considered a reliable synapomorphy of Eusuchia (Turner and Buckley 2008; Pol et al. 2009; Tennant et al. 2016; Pochat-Cottilloux et al. 2024). This complexity highlights the ongoing difficulty in providing a robust definition for Eusuchia and calls for a re-assessment of traditional character combinations in light of new fossil data and broader taxon sampling.

Atoposauridae is recovered as a well-supported monophyletic clade (Bremer support of 4), with a relatively stable internal topology similar to that retrieved by Pochat-Cottilloux et al. (2024), but better resolved. The node is defined by a combination of cranial and postcranial synapomorphies, including a broad oreinirostral rostrum, limited participation of the premaxilla in the internarial bar and a laterally open cranioquadrate passage that is not enclosed by the quadrate, squamosal and otoccipital. Additional diagnostic features include a reduced antorbital fenestra and two rows of dorsal osteoderms with a well-developed anterolateral process. Further synapomorphies are the presence of symmetrically compressed maxillary teeth and a posteriorly tapering lacrimal that either does not contact the jugal or does so only slightly. Unfortunately, the only one of these synapomorphies preserved in ML2631 is the laterally open cranioquadrate passage, which, in this case, is formed exclusively by the exoccipital. Nevertheless, the consistent recovery of ML2631 in a more deeply nested position than some other atoposaurids can be explained by the presence of several additional derived character states preserved in the specimen, some of which occur variably amongst other atoposaurids. The optimisation of these traits placed ML2631 on the branch between *Knoetschkesuchus* and *Sabresuchus*, whereas other taxa scored more extensively, including for plesiomorphic characters not preserved in ML2631, were recovered in more basal positions. This also accounts for the relatively low Bremer support obtained at some nodes within the group.

However, despite its fragmentary nature, the inclusion of ML2631 in the analysis has helped to resolve all polytomies within the clade Atoposauridae. In the analysis by Pochat-Cottilloux et al. (2024), the relationships amongst *Sabresuchus*, *Alligatorium* + *Theriosuchus*, *Knoetschkesuchus* and *Varanosuchus* + *Aprosuchus* remained unresolved. Following the inclusion of ML2631, the analysis recovers a topology in which two major sister clades are present within Atoposauridae. One includes *Alligatorium* and *Theriosuchus* and the other comprises *Sabresuchus*, *Knoetschkesuchus*, *Varanosuchus*, *Aprosuchus* and ML2631. Within this latter group, two additional sister clades are recovered: one formed by *Varanosuchus* and *Aprosuchus* and another composed of the successive sister taxa *Knoetschkesuchus langenbergensis* Schwarz, Raddatz & Wings, 2017, *Knoetschkesuchus guimarotae*, ML2631 and *Sabresuchus*. However, although fully resolved and lacking polytomies, internal support for the nodes within Atoposauridae remains very low, with Bremer values of 1 and bootstrap supports below 50%, except for the relationship between *Varanosuchus* and *Aprosuchus*, which is strongly supported (Bremer value of 6 and bootstrap support of 83%).

The clade formed by *Knoetschkesuchus* spp., ML2631 and *Sabresuchus sympiestodon* (Martin, Rabi & Csiki 2010) is characterised by the following synapomorphies: rod-shaped jugal bar beneath the infratemporal fenestra; completely septated choanal groove; presence of a mandibular fenestra; jugal extension below the orbit not exceeding the anterior margin of the orbit; posteromedially directed premaxilla–maxilla suture in palatal view, medial to the alveolar region; and frontal lateral margins flush with the skull surface. However, in ML2631 only the septated choanal groove and the flush orbital lateral margin could be coded. The clade formed by ML2631 and *S. sympiestodon* is supported by two synapomorphies: the bar between the orbit and the supratemporal fossa is narrow, with sculpting restricted to its anterior surface in mature specimens; and the choanal opening is posteriorly closed by an elevated wall formed by the pterygoids.

Finally, specimen ML2631 is characterised by an exclusive combination of two autapomorphies: the lateral margin of the squamosal bears a prominent depressed area just anterior to the posterior lobe, with a discontinuous groove for the ear valve; and the dorsal surface of the skull at the parietal–squamosal contact displays a distinct depression or sulcus. The presence of a discontinuous groove for the ear valve musculature is a feature commonly observed in paralligatorids, such as *Paralligator* and *Shamosuchus* (Turner 2015), but it has also been described in closely-related atoposaurids, such as *Aprosuchus* and *Varanosuchus* (Venczel and Codrea 2019; Pochat-Cottilloux et al. 2024). The same applies to the presence of a sulcus or depression in the parietal–squamosal suture region, which is also found in some paralligatorids, like *Wannchampsus* (Adams 2014) and in notosuchians, such as *Notosuchus* (Fiorelli and Calvo 2008; Barrios et al. 2017), as well as in other atoposaurids, like *Theriosuchus*, *Aprosuchus* and *Varanosuchus* (Venczel and Codrea 2019; Pochat-Cottilloux et al. 2024). However, as noted in the anatomical description, the condition of the latter character in ML2631 appears to differ slightly from that of the aforementioned taxa, as the sulcus is located in the posterior region of the supratemporal fossa and does not reach the posterior margin of the skull roof.

These results reinforce the phylogenetic significance of ML2631 and its value in refining atoposaurid relationships, despite its fragmentary preservation. The specimen not only contributes to resolving previously collapsed nodes within Atoposauridae, but also exhibits a unique combination of anatomical features that clearly distinguish it from other known atoposaurids. However, due to its incomplete nature, it is here retained in open nomenclature as Atoposauridae indet. until more complete material is available to confirm its status as a new taxon.

Comparisons within Atoposauridae

The fragmentary nature of ML2631 limits the scope of anatomical comparisons across Atoposauridae. Only the cranial table and most of the neurocranium are preserved, preventing direct evaluation of many characters typically used in atoposaurid systematics (e.g. dentition, preorbital morphology, palatal structure and osteoderms). However, the preserved elements retain several diagnostic and phylogenetically informative features that allow meaningful comparison with other members of the clade.

Atoposaurids are typically characterised by a combination of features, including small body size, brevirostrine and dorsoventrally compressed skulls, well-developed dermal ornamentation, relatively large orbits compared to skull length, relatively reduced supratemporal fenestrae and often heterodont dentition with conical, pseudocaniniform or lanceolate tooth morphologies. External mandibular fenestrae and short secondary choanae are also commonly reported within the clade (e.g. Buscalioni and Sanz (1988); Schwarz and Salisbury (2005); Tennant et al. (2016); Schwarz et al. (2017); Venczel and Codrea (2019); Pochat-Cottilloux et al. (2024)). Although most of these traits cannot be assessed in ML2631 due to the limited preservation of the specimen, several features of the cranial table and braincase reveal informative similarities and differences with other atoposaurids. In particular, the configuration of the supratemporal fenestrae, the morphology of the parietal–squamosal suture with a posterior sulcus bordering the fenestra, the arrangement of the sulcus associated with the ear valve musculature and the shape of the posterolateral margin of the squamosal appear to distinguish ML2631 from all currently known species.

The cranial table of ML2631 exhibits deep pits, forming a strongly marked ornamentation pattern (Fig. 4A). With the exception of the unsculpted skull of *Atoposaurus* or the subtle, shallow pits observed in *Alligatorellus*, this type of well-defined dermal ornamentation is common amongst atoposaurids and is generally regarded as a typical feature of the group (Tennant et al. 2016; Schwarz et al. 2017; Pochat-Cottilloux et al. 2024). However, this character must be interpreted with caution, as the intensity and development of skull table ornamentation can vary with ontogenetic stage. In *Knoetschkesuchus langenbergensis*, for example, larger individuals display deeply pitted skull tables, while smaller specimens lack or exhibit only faint ornamentation (Schwarz et al. 2017). Similarly, in *Aprosuchus ghirai*, the presence of dense sculpturing has been interpreted as indicative of a subadult condition (Venczel and Codrea 2019).

Regarding other structures on the skull table, a distinct mid-line ridge is present on both the frontal and the parietal in ML2631, although it is more subtle and restricted to the posterior half in the frontal (Fig. 4A). This condition has been frequently reported amongst atoposaurids and related neosuchians, but with notable variation across taxa and ontogenetic stages. In *Theriosuchus*, a mid-line frontal ridge has often been considered diagnostic (Schwarz and Salisbury 2005; Salisbury and Naish 2011; Tennant et al. 2016). However, its development appears to be ontogenetically dependent: in *Knoetschkesuchus guimarotae*, the ridge is absent in smaller individuals and becomes more developed in larger ones, where it may overgrow the median suture (Schwarz and Salisbury 2005). In *K. langenbergensis*, the parietal is incompletely fused and lacks any dorsal crest, maintaining a flat surface (Schwarz et al. 2017). A sagittal crest on the frontal and parietal has also been reported in *Varanosuchus wangleeorum*, *Aprosuchus ghirai* and *Sabresuchus sympiestodon* (Martin et al. 2014; Venczel and Codrea 2019; Pochat-Cottilloux et al. 2024). The condition observed in ML2631, with a well-defined crest on the parietal and a weaker, posteriorly limited ridge on the frontal, falls within the morphological variability documented in other atoposaurids. Additionally, a similar sagittal ridge is present in paralligatorids, such as *Shamosuchus* (Pol et al. 2009) and *Wannchampsus* (Adams 2014), as well as in some notosuchians (Martin et al. 2014; Tennant et al. 2016).

The size of the supratemporal fenestrae in relation to the width of the interfenestral bar formed by the frontal and parietal, is a relevant character for comparison. These two aspects are functionally and morphologically related, as larger fenestrae logically correlate with a narrower interfenestral bar and vice versa. In ML2631, the supratemporal fenestrae are relatively large, being approximately twice as wide as the interfenestral bar and they are slightly elongated in the anteroposterior direction (Fig. 4A). Amongst other atoposaurids, this character shows considerable variation. Taxa with larger supratemporal fenestrae, such as *Knoetschkesuchus guimarotae* (Schwarz and Salisbury 2005), *Theriosuchus pusillus* (Tennant et al. 2016) and *Sabresuchus sympiestodon* (Martin et al. 2014), display a narrow interfenestral bar similar to that of ML2631. However, in *K. guimarotae*, the fenestrae appear to be more quadrangular rather than elliptical, based on the reconstruction by Schwarz and Salisbury (2005). In contrast, taxa with smaller and more anteroposteriorly elongated fenestrae, such as *Alligatorellus* (Tennant et al. 2016), *Knoetschkesuchus langenbergensis* (Schwarz et al. 2017) and *Aprosuchus* (Venczel and Codrea 2019), have a much broader interfenestral bar. Notably, *Alligatorellus* also differs in having a closed internal supratemporal fenestra, a condition not observed in other atoposaurids (Tennant et al. 2016). Other taxa, such as *Varanosuchus* (Pochat-Cottilloux et al. 2024) and *Alligatorium* (Tennant et al. 2016), seem to exhibit an intermediate condition. It should also be noted that comparisons of this feature between specimens of significantly different sizes or ontogenetic stages should be approached with caution, as the relationship between the size of the supratemporal fenestrae and the width of the interfenestral bar appears to have an ontogenetic component (Venczel and Codrea 2019). In species for which individuals of different sizes are known, such as *Theriosuchus pusillus* or *Knoetschkesuchus langenbergensis*, the fenestrae tend to become relatively larger

and less anteroposteriorly elongated in larger individuals (Tennant et al. 2016; Schwarz et al. 2017), a pattern that is generally widespread amongst crocodylomorphs.

Comparison of the supratemporal fenestrae with the orbits is more difficult, as only the posteromedial margin of the orbital rim is preserved, but it is nonetheless evident that the orbit would have been substantially larger than the fenestra. However, part of the frontal between the orbits is preserved, allowing an estimate of the interorbital width. In ML2631, the interorbital and interfenestral widths are nearly equal (subequal), with the interfenestral bar being only slightly wider (Fig. 4A). The relative width of these two regions is a useful comparative feature amongst atoposaurids (Tennant et al. 2016). This proportion in ML2631 closely resembles the condition observed in *Sabresuchus sympiestodon*, where both widths are subequal, with a minimally broader interfenestral bar (Martin et al. 2010, 2014). In contrast, other atoposaurids such as *Knoetschkesuchus langenbergensis* (Schwarz et al. 2017) and *Aprosuchus ghirai* (Venczel and Codrea 2019) also exhibit a greater interfenestral width, but the difference relative to the interorbital region is more evident. A similar condition is found in *Alligatorellus beaumonti* Gervais, 1871 and *Montsecosuchus depereti* (Vidal, 1915), where the interfenestral width clearly exceeds the interorbital one (Buscalioni and Sanz 1990; Tennant et al. 2016). In *Knoetschkesuchus guimarotae*, both widths are narrow and nearly equal (Schwarz and Salisbury 2005). On the contrary, in *Varanosuchus* (Pochat-Cottilloux et al. 2024), *Alligatorium meyeri* Gervais, 1871 and *Theriosuchus pusillus*, the interorbital width exceeds the interfenestral one (Tennant et al. 2016). According to Tennant et al. (2016), these proportional differences do not appear to be solely ontogenetically driven, as many specimens with differing configurations show signs of skeletal maturity. Thus, the interorbital–interfenestral relationship displays meaningful variation within Atoposauridae and may carry phylogenetic or functional significance.

A distinct anteromedially orientated sulcus is present on the dorsal surface of both postorbitals in ML2631 (Fig. 4A). This structure corresponds to the ventral depression or shallow groove described on the dorsal margin of the postorbital in other neosuchians (Tennant et al. 2016). Within Atoposauridae, this feature is clearly present in *Alligatorellus* and possibly in *Alligatorium meyeri* and has, therefore, been proposed as diagnostic for the clade. Conversely, it appears to be absent in *Theriosuchus pusillus* and is of uncertain presence in *Knoetschkesuchus* (Tennant et al. 2016) and *Varanosuchus* (Pochat-Cottilloux et al. 2024). In *Aprosuchus ghirai*, a transverse bony ridge divides the dorsal surface of the postorbital into anterior and posterior depressed regions (Venczel and Codrea 2019), potentially reflecting a related structural configuration. A comparable postorbital groove or depression has also been documented in some paralligatorids, including *Paralligator gradilifrons* Konzhukova, 1954, the Glen Rose Form and *Wannchampsus* (Adams 2014; Turner 2015; Tennant et al. 2016), as well as in more basal crocodyliforms, such as the shartegosuchid *Fruitachampsa callisoni* (Clark 2011). The presence of this feature in ML2631 supports its attribution to Atoposauridae and adds to the growing evidence of its wider distribution within Neosuchia.

The cranioquadrate passage in ML2631 appears dorsolaterally open (Fig. 4C), with no evident contact between the quadrate, squamosal and exoccipital to form a fully enclosed canal. Instead, the exoccipital alone seems to define the medial, ventral and most of the lateral margins of the open passage. This condition closely resembles that observed in *Varanosuchus*, where the canal also appears as an open groove in lateral view, formed solely by the exoccipital (Pochat-Cottilloux et al. 2024). A comparable configuration is reported in *Knoetschkesuchus langenbergensis* and *Sabresuchus sympiestodon*, both of which exhibit an unroofed cranioquadrate canal (Schwarz et al. 2017; Venczel and Codrea 2019). In contrast, *Knoetschkesuchus guimarotae* (Schwarz and Salisbury 2005) and *Aprosuchus ghirai* show a completely enclosed canal due to contact between the quadrate and squamosal (Venczel and Codrea 2019). Amongst other atoposaurids, an open cranioquadrate passage has also been described in *Alligatorium* and *Alligatorellus* and is, therefore, considered a diagnostic feature of the clade (Tennant et al. 2016). An open cranioquadrate passage or *canalis quadratosquamosoexoccipitalis*, lacking a lateral wall, is also present in several other neosuchian clades, such as Goniopholididae, Pholidosauridae and eusuchians, like Allodaposuchidae (e.g. Salisbury (1999); Delfino et al. (2008); Puértolas-Pascual et al. (2014); Tennant et al. (2016)). In contrast, other neosuchians, such as Susisuchidae and extant crocodylians, possess a fully enclosed passage formed by the exoccipital and quadrate (e.g. Salisbury et al. (2006); Pol et al. (2009)). The condition seen in ML2631 thus supports its placement within Atoposauridae and contributes to the broader understanding of cranioquadrate canal evolution within Neosuchia.

A slightly elevated parietal rim borders the medial margin of the supratemporal fenestrae in ML2631 (Fig. 4A). This ridge is particularly well defined along the posteromedial and medial margins, but appears absent on the anteromedial border, which is formed by the frontal. This partial elevation contrasts with the condition observed in most atoposaurids, where the supratemporal rim is well developed along the entire medial margin of both the parietal and frontal. For instance, *Alligatorium*, *Theriosuchus*, *Varanosuchus*, *Knoetschkesuchus guimarotae* and *Sabresuchus* all exhibit a dorsally elevated rim extending the full medial border of each fenestra (Tennant et al. 2016; Pochat-Cottilloux et al. 2024). In contrast, *Alligatorellus beaumonti* possesses a ridge that is only developed posteriorly, showing a condition similar to that of ML2631. Conversely, in *Alligatorellus bavaricus* Wellnhofer, 1971, *Montsecosuchus* and *Knoetschkesuchus langenbergensis*, the medial margins remain flat (Tennant et al. 2016; Schwarz et al. 2017).

In ML2631, the supraoccipital is primarily visible in occipital view, contributing only slightly to the dorsal surface of the skull table (Fig. 4A$_2$). This condition contrasts with that observed in *Alligatorellus*, where the posterodorsal margins of the parietals and squamosals completely cover the occipital region, excluding the supraoccipital from the dorsal skull surface, a feature initially considered autapomorphic for the genus (Tennant et al. 2016). In ML2631, as in many other mesoeucrocodylians, the supraoccipital remains at least partially exposed dorsally, reflecting a more generalised neosuchian condition.

In ML2631, only the left supratemporal fenestra is preserved. Its posterior region is marked by a distinct fossa that extends posteriorly around the parietal–squamosal suture, although it does not reach the posterior margin of the skull table (Fig. 4A). This contrasts with the condition in *Theriosuchus pusillus*, where the posterior sulcus along the squamosal–parietal suture, bounded by elevated rims, appears to reach the posterior edge of the skull roof (Tennant et al. 2016). A comparable posterior sulcus is described in *Alligatorellus*, originating as a shallow groove at the parietal–squamosal contact and continuing into the fenestra (Tennant et al. 2016). In *Varanosuchus*, the parietal–squamosal suture is raised and grooved, although no fossa like the one in ML2631 is present along the posterior margin of the supratemporal fenestra (Pochat-Cottilloux et al. 2024). In *Alligatorellus beaumonti* and *Alligatorium meyeri*, the groove is flanked by low ridges, whereas in *Montsecosuchus* and *Knoetschkesuchus*, the suture is flat and ungrooved, lacking any posterior depression (Tennant et al. 2016; Schwarz et al. 2017). A sulcus or depression in the parietal–squamosal region is also present in some paralligatorids, such as *Wannchampsus* (Adams 2014) and in notosuchians, like *Notosuchus* (Fiorelli and Calvo 2008; Barrios et al. 2017). Although several atoposaurids exhibit varying degrees of development of a longitudinal sulcus with elevated margins along the squamosal–parietal suture, the condition observed in ML2631, with a broader and well-defined fossa posterior to the supratemporal fenestra that does not reach the posterior skull margin, appears to be unique amongst Neosuchia.

In ML2631, the squamosal lobe is poorly preserved, but the available evidence suggests a flat posterolateral margin that is unsculptured and lies in line with the general level of the skull table, with no clear step or ventral deflection (Fig. 4A, C). This contrasts with the condition in many atoposaurids and paralligatorids, where the squamosal lobe is offset ventrally, creating a step-like depression relative to the skull table, as seen in *Theriosuchus pusillus*, *Sabresuchus ibericus* (Brinkmann, 1992), *Knoetschkesuchus* or the paralligatorids *Shamosuchus* and *Rugosuchus* (Pol et al. 2009; Tennant et al. 2016; Schwarz et al. 2017). *Aprosuchus ghirai* also exhibits a bevelled, ventrally directed squamosal lobe that is unsculptured and accompanied by a deep, anteriorly extending groove for the upper ear lid musculature, with its lower margin laterally displaced (Venczel and Codrea 2019). Conversely, *Alligatorium meyeri* and *Alligatorellus beaumonti* display a squamosal lobe aligned with the cranial table, although unsculptured, whereas in *Alligatorellus bavaricus* the lobe is absent altogether (Tennant et al. 2016). In ML2631, a subtle lateral peak is present along the concave lateral squamosal edge, coinciding with a short, discontinuous groove for the ear valve musculature. A comparable configuration, either a discontinuous or medially curved lateral groove, has been reported in *Alligatorium meyeri*, *Aprosuchus*, *S. ibericus*, some specimens of *Varanosuchus* and paralligatorids, such as *Shamosuchus* and *Paralligator* (Pol et al. 2009; Tennant et al. 2016; Pochat-Cottilloux et al. 2024). The morphology of ML2631 thus appears intermediate, with no clear evidence of ventral displacement of the lobe, but showing traits, such as an unsculptured lateral surface and a discontinuous groove that are shared with both atoposaurids and paralligatorids.

In ML2631, the internal choana is positioned within a pronounced depression in the ventral surface of the pterygoids and appears elongate, bordered posteriorly by a raised wall, while the lateral margins are more gently sloped and poorly defined (Fig. 4B). It is clearly divided by a narrow vertical septum. Although preservation limits a full assessment, the choanal aperture is wide and situated near the posterior margin of the pterygoid, suggesting a relatively posterior placement. This condition contrasts with that seen in *Knoetschkesuchus guimarotae* and *K. langenbergensis*, where the choana is more anteriorly positioned, slit-like and only weakly set within a shallow groove rather than a well-defined depression (Schwarz et al. 2017). In *Theriosuchus pusillus*, the choana is more deeply inset into the pterygoids, located anterior to the posterior margin of the suborbital fenestrae and only partially divided by a septum (Tennant et al. 2016). In *Aprosuchus ghirai*, the choana is described as relatively large, oval and partially separated by a mid-line septum, positioned close to the posterior edge of the suborbital fenestrae (Venczel and Codrea 2019), while, in *Varanosuchus*, they are ovoid, entirely enclosed by the pterygoids and lack a septum (Pochat-Cottilloux et al. 2024). The condition in ML2631, with a choana posteriorly placed within a deep depression, a vertically orientated posterior pterygoid wall and a distinct septum, more closely resembles that of *T. pusillus* and *Aprosuchus* than that of *Knoetschkesuchus* or *Varanosuchus*, though the precise anterior extent and palatine contribution remain unclear.

In summary, although ML2631 preserves only a limited portion of the skull, its combination of features, including a dorsolaterally open cranioquadrate passage, a posteriorly placed and septate internal choana, a partially elevated supratemporal rim, large supratemporal fenestrae with a distinct posterior fossa and a squamosal lobe with a discontinuous groove, does not match any currently known atoposaurid species. These characters suggest that ML2631 represents a potentially distinct and informative new taxon within Atoposauridae. However, further discoveries and more complete material will be necessary to confirm its taxonomic distinctiveness and refine its placement within the clade.

Conclusions

Specimen ML2631, discovered in the Zimbral VMA (Lourinhã Formation, Upper Jurassic, Portugal), represents the first atoposaurid crocodylomorph for which neuroanatomical structures and neurosensorial capabilities have been reconstructed and estimated using micro-computed tomography (μCT). Although fragmentary, the specimen preserves significant portions of the skull table and braincase, revealing a unique combination of anatomical traits not previously documented within Atoposauridae. Notable characteristics include a dorsolaterally open cranioquadrate passage, sagittal crests along the frontal and parietal bones, large supratemporal fenestrae with distinct posterior fossae, a posteriorly positioned septate choana and a discontinuous groove on the squamosal lobe. These morphological features appear to distinguish ML2631 from other known atoposaurids and suggest it may represent a novel taxon.

The neuroanatomical analysis, including detailed reconstructions of the brain endocast, inner ear, cranial nerves and paratympanic sinus system, provides new insights into the sensory palaeobiology and ecological adaptations of atoposaurids. The morphology of the endosseous labyrinth, particularly the tall anterior semicircular canal and slender crus commune, suggests good angular sensitivity and balance control, probably indicating well-developed terrestrial locomotion capabilities. Nevertheless, certain features such as moderate canal thickness and labyrinth proportions remain consistent with semi-aquatic or nearshore habitats. The relatively short cochlear duct indicates sensitivity to low-frequency auditory stimuli, likely facilitating the detection of environmental sounds like water movements or distant calls. Furthermore, despite the reduced body size of the specimen (~ 0.8 m), the relatively small mesencephalic volume resembles the condition seen in large, mature crocodylians, supporting the interpretation of ML2631 as an adult dwarf individual with moderate visual acuity, consistent with a terrestrial to semi-aquatic lifestyle.

Phylogenetic analyses clearly position ML2631 within Atoposauridae, substantially clarifying previously uncertain relationships within the clade (Pochat-Cottilloux et al. 2024). Its inclusion resolves prior polytomies, grouping ML2631 with taxa such as *Sabresuchus* and *Knoetschkesuchus*, a position consistent with its stratigraphic age and European palaeobiogeography. Despite a significant ghost lineage between the Late Jurassic atoposaurids and the Late Cretaceous taxa, such as *Sabresuchus sympiestodon*, isolated teeth and fragmentary material assigned to atoposaurids are common in Lower Cretaceous deposits (e.g. Brinkmann (1992); Buscalioni et al. (2008); Puértolas-Pascual et al. (2015)), indicating the persistence of this group throughout the Cretaceous, although few species have been described. Despite low support values at several nodes, the resulting topology emphasises the phylogenetic informativeness of ML2631. However, due to its incomplete preservation, ML2631 is provisionally designated as Atoposauridae indet. Further discoveries of more complete cranial and postcranial materials from similar stratigraphic contexts will be essential to test its potential taxonomic status as a new species and refine its phylogenetic position.

Overall, ML2631 highlights the importance of even fragmentary specimens for advancing our understanding of anatomical diversity, ecological adaptations and evolutionary relationships within Crocodylomorpha, in general and Atoposauridae, in particular. This work emphasises the utility of integrating modern digital imaging and palaeoneurological techniques with traditional comparative anatomy and phylogenetic analyses to extract critical data from limited fossil remains.

Acknowledgements

This work was funded by the MiCrocs project: Programa de Incentivo à Investigação Horácio Mateus (PIIHM), funded by the Grupo de Etnologia e Arqueologia da Lourinhã (GEAL). E.P.-P. was supported by a postdoctoral grant funded by the Fundação para a Ciência e a Tecnologia, Portugal (SFRH/BPD/116759/2016) and by a postdoctoral contract (María Zambrano) funded by the Ministry of Universities of the Government of Spain through the Next Generation EU funds of the European Union. Thanks to Pedro Aquino, Flávio Domingues and Tiago Ferreira (Micronsense, Metrologia Industrial, Lda., Leiria, Portugal) for conducting the micro-CT scan. I also want to acknowledge the work of Micael Martinho and Carla Alexandra Tomás for their contribution to the finding and preparation of the fossil specimen. Special thanks are extended to the two anonymous reviewers and the editor for their constructive comments and suggestions, which helped improve the quality of this manuscript.

References

Adams TL (2014) Small crocodyliform from the Lower Cretaceous (Late Aptian) of Central Texas and its systematic relationship to the evolution of Eusuchia. Journal of Paleontology 88(5): 1031–1049. https://doi.org/10.1666/12-089

Alves TM, Manuppella G, Gawthorpe RL, Hunt DW, Monteiro JH (2003) The depositional evolution of diapir- and fault-bounded rift basins: examples from the Lusitanian Basin of West Iberia. Sedimentary Geology 162(3–4): 273–303. https://doi.org/10.1016/S0037-0738(03)00155-6

Barrios F, Bona P, Paulina-Carabajal A, Gasparini Z (2018) Re-description of the cranio-mandibular anatomy of *Notosuchus terrestris* (Crocodyliformes, Mesoeucrocodylia) from the Upper Cretaceous of Patagonia. Cretaceous Research 83: 3–39. https://doi.org/10.1016/j.cretres.2017.08.016

Barrios F, Bona P, Paulina-Carabajal A, Leardi JM, Holliday CM, Lessner EJ (2022) An overview on the Crocodylomorpha cranial neuroanatomy: variability, morphological patterns and paleobiological implications. In: Dozo MT, Paulina-Carabajal A, Macrini

TE, Walsh S (Eds) Paleoneurology of amniotes: New directions in the study of fossil endocasts. Springer, Cham, 213–266. https://doi.org/10.1007/978-3-031-13983-3_7

Benton MJ, Clark JM (1988) Archosaur phylogeny and the relationships of the Crocodylia. In: Benton MJ (Ed.) The phylogeny and classification of the tetrapods, Vol. 1: Amphibians, Reptiles, Birds. Systematics Association Special Vol. 35A. Clarendon Press, Oxford, 295–338.

Bona P, Degrange FJ, Fernández MS (2013) Skull anatomy of the bizarre crocodylian *Mourasuchus nativus* (Alligatoridae, Caimaninae). The anatomical record 296(2): 227–239. https://doi.org/10.1002/ar.22625

Bona P, Carabajal AP, Gasparini Z (2017) Neuroanatomy of *Gryposuchus neogaeus* (Crocodylia, Gavialoidea): a first integral description of the braincase and endocranial morphological variation in extinct and extant gavialoids. Earth and Environmental Science Transactions of the Royal Society of Edinburgh 106(4): 235–246. https://doi.org/10.1017/S1755691016000189

Brinkmann W (1992) Die Krokodilier-Fauna aus der Unter-Kreide (Ober-Barremium) von Uña (Provinz Cuenca, Spanien). Berliner Geowissenschaftliche Abhandlungen (E) 5: 1–123.

Brown B (1933) An ancestral crocodile. American Museum Novitates 638: 1–4.

Brown CH, Waser PM (1984) Hearing and communication in blue monkeys (*Cercopithecus mitis*). Animal behaviour 32(1): 66–75. https://doi.org/10.1016/S0003-3472(84)80325-5

Brusatte SL, Muir A, Young MT, Walsh S, Steel L, Witmer LM (2016) The braincase and neurosensory anatomy of an Early Jurassic marine crocodylomorph: implications for crocodylian sinus evolution and sensory transitions. The Anatomical Record 299(11): 1511–1530. https://doi.org/10.1002/ar.23462

Buscalioni AD, Sanz JL (1988) Phylogenetic relationships of the Atoposauridae (Archosauria, Crocodylomorpha). Historical Biology 1(3): 233–250. https://doi.org/10.1080/08912968809386477

Buscalioni AD, Sanz JL (1990) *Montsecosuchus depereti* (Crocodylomorpha, Atoposauridae), new denomination for *Alligatorium depereti* Vidal, 1915 (Early Cretaceous, Spain): redescription and phylogenetic relationships. Journal of Vertebrate Paleontology 10(2): 244–254. https://doi.org/10.1080/02724634.1990.10011840

Buscalioni AD, Ortega F, Pérez-Moreno BP, Evans SE (1996) The Upper Jurassic maniraptoran theropod *Lisboasaurus estesi* (Guimarota, Portugal) reinterpreted as a crocodylomorph. Journal of Vertebrate Paleontology 16(2): 358–362. https://doi.org/10.1080/02724634.1996.10011322

Buscalioni AD, Fregenal MA, Bravo A, Poyato-Ariza FJ, Sanchíz B, Báez AM, Cambra-Moo O, Martín-Closas C, Evans SE, Lobón JM (2008) The vertebrate assemblage of Buenache de la Sierra (Upper Barremian of Serrania de Cuenca, Spain) with insights into its taphonomy and palaeoecology. Cretaceous Research 29(4): 687–710. https://doi.org/10.1016/j.cretres.2008.02.004

Buscalioni AD, Alcalá L, Espílez E, Mampel L (2013) European Goniopholididae from the Early Albian Escucha Formation in Ariño (Teruel, Aragón, Spain). Spanish Journal of Palaeontology 28(1): 103–122. https://doi.org/10.7203/sjp.28.1.17835

Clark JM (1986) Phylogenetic relationships of the crocodylomorph archosaurs. PhD Thesis, The University of Chicago, Chicago, USA.

Clark JM (2011) A new shartegosuchid crocodyliform from the Upper Jurassic Morrison Formation of western Colorado. Zoological Journal of the Linnean Society 163(suppl_1): S152–S172. https://doi.org/10.1111/j.1096-3642.2011.00719.x

Costa F, Mateus O (2019) Dacentrurine stegosaurs (Dinosauria): A new specimen of *Miragaia longicollum* from the Late Jurassic of Portugal resolves taxonomical validity and shows the occurrence of the clade in North America. PLoS ONE 14(11): e0224263. https://doi.org/10.1371/journal.pone.0224263

Delfino M, Codrea V, Folie A, Dica P, Godefroit P, Smith T (2008) A complete skull of *Allodaposuchus precedens* Nopcsa, 1928 (Eusuchia) and a reassessment of the morphology of the taxon based on the Romanian remains. Journal of Vertebrate Paleontology 28(1): 111–122. https://doi.org/10.1671/0272-4634(2008)28%5B111:ACSOAP%5D2.0.CO;2

Dodson P (1975) Functional and ecological significance of relative growth in *Alligator*. Journal of Zoology 175(3): 315–355. https://doi.org/10.1111/j.1469-7998.1975.tb01405.x

Dufeau DL, Witmer LM (2015) Ontogeny of the middle-ear air-sinus system in *Alligator mississippiensis* (Archosauria: Crocodylia). PLoS ONE 10(9): e0137060. https://doi.org/10.1371/journal.pone.0137060

Dumont Jr MV, Santucci RM, de Andrade MB, de Oliveira CEM (2022) Paleoneurology of *Baurusuchus* (Crocodyliformes: Baurusuchidae), ontogenetic variation, brain size, and sensorial implications. The Anatomical Record 305(10): 2670–2694. https://doi.org/10.1002/ar.24567

Eijkelboom I (2020) Postcranial remains of *Knoetschkesuchus guimarotae* (Atoposauridae, Crocodylomorpha) from the Late Jurassic of Portugal and its locomotor behaviour. MSc Thesis, Utrecht University, The Netherlands.

Erb A, Turner AH (2021) Braincase anatomy of the Paleocene crocodyliform *Rhabdognathus* revealed through high resolution computed tomography. PeerJ 9: e11253. https://doi.org/10.7717/peerj.11253

Erickson BR (1976) Osteology of the early eusuchian crocodile *Leidyosuchus formidabilis*, sp. nov. Monograph of the Science Museum of Minnesota Paleontology 2: 1–61.

Fernandes AE, Beccari V, Kellner AW, Mateus O (2023) A new gnathosaurine (Pterosauria, Archaeopterodactyloidea) from the Late Jurassic of Portugal. PeerJ 11: e16048. https://doi.org/10.7717/peerj.16048

Fiorelli LE, Calvo J (2008) New remains of *Notosuchus terrestris* Woodward, 1896 (Crocodyliformes: Mesoeucrocodylia) from Late Cretaceous of Neuquén, Patagonia, Argentina. Arquivos do Museu Nacional, Rio de Janeiro 66(1): 83–124.

Garrick LD, Lang JW (1977) Social signals and behaviors of adult alligators and crocodiles. American Zoologist 17(1): 225–239. https://doi.org/10.1093/icb/17.1.225

Gervais P (1871) Remarques au sujet des Reptiles provenant des calcaires lithographiques de Cerin, dans le Bugey, qui sont conservés au Musée de Lyon. Comptes Rendus des séances de l'Academie de Sciences 73: 603–607.

Goloboff PA (1999) Analyzing large data sets in reasonable times: solutions for composite optima. Cladistics 15(4): 415–428. https://doi.org/10.1111/j.1096-0031.1999.tb00278.x

Goloboff PA, Morales ME (2023) TNT version 1.6, with a graphical interface for MacOS and Linux, including new routines in parallel. Cladistics 39(2): 144–153. https://doi.org/10.1111/cla.12524

Guillaume ARD (2024) Albanerpetontidae (Lissamphibia) and other small herpetofauna (Crocodylomorpha, Lepidosauria, Choristodera) from the Iberian Mesozoic, with focus on the Upper Jurassic of Portugal. PhD Thesis, Universidade Nova de Lisboa, Caparica, Portugal.

Guillaume AR, Moreno-Azanza M, Puértolas-Pascual E, Mateus O (2020) Palaeobiodiversity of crocodylomorphs from the Lourinhã Formation based on the tooth record: insights into the palaeoecology of the Late Jurassic of Portugal. Zoological Journal of the Linnean Society 189(2): 549–583. https://doi.org/10.1093/zoolinnean/zlz112

Guillaume AR, Natário C, Mateus O, Moreno-Azanza M (2023) Plasticity in the morphology of the fused frontals of Albanerpetontidae (Lissamphibia; Allocaudata). Historical Biology 35(4): 537–554. https://doi.org/10.1080/08912963.2022.2054712

Hay O (1930) Second Bibliography and Catalogue of the Fossil Vertebrata of North America 2. Carnegie Institution of Washington, Washington, D.C.

Herrera Y, Leardi JM, Fernández MS (2018) Braincase and endocranial anatomy of two thalattosuchian crocodylomorphs and their relevance in understanding their adaptations to the marine environment. PeerJ 6: e5686. https://doi.org/10.7717/peerj.5686

Holliday CM, Witmer LM (2009) The epipterygoid of crocodyliforms and its significance for the evolution of the orbitotemporal region of eusuchians. Journal of Vertebrate Paleontology 29(3): 715–733. https://doi.org/10.1671/039.029.0330

Hurlburt G (1999) Comparison of body mass estimation techniques, using recent reptiles and the pelycosaur *Edaphosaurus boanerges*. Journal of Vertebrate Paleontology 19(2): 338–350. https://doi.org/10.1080/02724634.1999.10011145

Iordansky NN (1973) The skull of Crocodilia. In: Gans C, Parsons TS (Eds) Biology of the Reptilia, Vol. 4: morphology. Academic Press, New York, 201–264.

Jirak D, Janacek J (2017) Volume of the crocodilian brain and endocast during ontogeny. PLoS ONE 12(6): e0178491. https://doi.org/10.1371/journal.pone.0178491

Jouve S (2007) Taxonomic revision of the dyrosaurid assemblage (Crocodyliformes: Mesoeucrocodylia) from the Paleocene of the Iullemmeden Basin, West Africa. Journal of Paleontology 81(1): 163–175. https://doi.org/10.1666/0022-3360(2007)81[163:TROTDA]2.0.CO;2

Jouve S, Bouya B, Amaghzaz M (2005) A short-snouted dyrosaurid (Crocodyliformes, Mesoeucrocodylia) from the Palaeocene of Morocco. Palaeontology 48(2): 359–369. https://doi.org/10.1111/j.1475-4983.2005.00442.x

Jouve S, Iarochene M, Bouya B, Amaghzaz M (2006) A new species of *Dyrosaurus* (Crocodylomorpha, Dyrosauridae) from the early Eocene of Morocco: phylogenetic implications. Zoological Journal of the Linnean Society 148(4): 603–656. https://doi.org/10.1111/j.1096-3642.2006.00241.x

Kley NJ, Sertich JJ, Turner AH, Krause DW, O'Connor PM, Georgi JA (2010) Craniofacial morphology of *Simosuchus clarki* (Crocodyliformes: Notosuchia) from the late Cretaceous of Madagascar. Journal of Vertebrate Paleontology 30(sup1): 13–98. https://doi.org/10.1080/02724634.2010.532674

Konzhukov,a ED (1954) New fossil crocodilians from Mongolia. Trudy Paleontologicheskogo Instituta ANSSSR 48: 171–194.

Krebs B (1967) Der Jura-Krokodilier *Machimosaurus* H. v. Meyer. Paläontologische Zeitschrift 41: 46–59. https://doi.org/10.1007/BF02998548

Krebs B (1968) Le Crocodilien *Machimosaurus*. Memorias do Serviços Geologicos de Portugal 41: 21–53.

Kullberg JC (2000) Evolução tectónica mesozóica da Bacia Lusitaniana. PhD Thesis, Universidade Nova de Lisboa, Caparica, Portugal.

Kullberg JC, Rocha RB, Soares AF, Duarte LV, Marques JF (2014) Palaeogeographical evolution of the Lusitanian Basin (Portugal) during the Jurassic. Part I: The tectonic constraints and sedimentary response. In: Rocha R, Pais J, Kullberg JC, Finney S (Eds) STRATI 2013, Springer Geology, 665–672. https://doi.org/10.1007/978-3-319-04364-7_127

Kuzmin IT, Boitsova EA, Gombolevskiy VA, Mazur EV, Morozov SP, Sennikov AG, Skutschas PP, Sues HD (2021) Braincase anatomy of extant Crocodylia, with new insights into the development and evolution of the neurocranium in crocodylomorphs. Journal of Anatomy 239(5): 983–1038. https://doi.org/10.1111/joa.13490

Leinfelder RR, Wilson RCL (1998) Third order sequences in an Upper Jurassic rift-related second order sequence, Central Lusitanian Basin, Portugal. In: de Graciansky P-C, Hardenbol J, Jacquin T, Vail P (Eds) Mesozoic and Cenozoic sequence stratigraphy of European basins. SEPM Special Publication 60, 507–525. https://doi.org/10.2110/pec.98.02.0507

Leite KJ, Fortier DC (2018) The palate and choanae structure of the *Susisuchus anatoceps* (Crocodyliformes, Eusuchia): phylogenetic implications. PeerJ 6: e5372. https://doi.org/10.7717/peerj.5372

Lessner EJ, Holliday CM (2022) A 3D ontogenetic atlas of *Alligator mississippiensis* cranial nerves and their significance for comparative neurology of reptiles. The Anatomical Record 305(10): 2854–2882. https://doi.org/10.1002/ar.24550

López-Rojas V, Mateus S, Marinheiro J, Mateus O, Puértolas-Pascual E (2024) A new goniopholidid crocodylomorph from the Late Jurassic of Portugal. Electronic Palaeontology 27(1): a5. https://doi.org/10.26879/1316

Narváez I, Brochu CA, Escaso F, Pérez-García A, Ortega F (2015) New crocodyliforms from southwestern Europe and definition of a diverse clade of European Late Cretaceous basal eusuchians. PLoS ONE 10(11): e0140679. https://doi.org/10.1371/journal.pone.0140679

Martin JE, Rabi M, Csiki Z (2010) Survival of *Theriosuchus* (Mesoeucrocodylia: Atoposauridae) in a Late Cretaceous archipelago: a new species from the Maastrichtian of Romania. Naturwissenschaften 97(9): 845–854. https://doi.org/10.1007/s00114-010-0702-y

Martin JE, Rabi M, Csiki-Sava Z, Vasile Ş (2014) Cranial morphology of *Theriosuchus sympiestodon* (Mesoeucrocodylia, Atoposauridae) and the widespread occurrence of *Theriosuchus* in the Late Cretaceous of Europe. Journal of Paleontology 88(3): 444–456. https://doi.org/10.1666/13-106

Martin JE, Smith T, Salaviale C, Adrien J, Delfino M (2020) Virtual reconstruction of the skull of *Bernissartia fagesii* and current understanding of the neosuchian–eusuchian transition. Journal of Systematic Palaeontology 18(13): 1079–1101. https://doi.org/10.1080/14772019.2020.1731722

Martinius AW, Gowland S (2011) Tide-influenced fluvial bedforms and tidal bore deposits (late Jurassic Lourinhã Formation, Lusitanian Basin, Western Portugal). Sedimentology 58(1): 285–324. https://doi.org/10.1111/j.1365-3091.2010.01185.x

Mateus O, Dinis J, Cunha PP (2017) The Lourinhã Formation: the Upper Jurassic to lower most Cretaceous of the Lusitanian Basin, Portugal–landscapes where dinosaurs walked. Ciências da Terra/Earth Sciences Journal 19(1): 75–97. https://doi.org/10.21695/cterra/esj.v19i1.355

Mateus O, Puértolas-Pascual E, Callapez PM (2019) A new eusuchian crocodylomorph from the Cenomanian (Late Cretaceous) of Portugal reveals novel implications on the origin of Crocodylia. Zoological Journal of the Linnean Society 186(2): 501–528. https://doi.org/10.1093/zoolinnean/zly064

Milner AR, Evans SE (1991) The upper Jurassic diapsid *Lisboasaurus estesi*. A maniraptoran theropod. Palaeontology 34(3): 503–513.

Nixon KC (1999) The parsimony ratchet, a new method for rapid parsimony analysis. Cladistics 15(4): 407–414. https://doi.org/10.1111/j.1096-0031.1999.tb00277.x

Owen R (1879) Monograph on the fossil Reptilia of the Wealden and Purbeck formations. Supplement No. IX. Crocodilia (*Goniopholis*, *Brachydectes*, *Nannosuchus*, *Theriosuchus* and *Nuthetes*).

Monograph of the Palaeontographical Society 33: 1–15. https://doi.org/10.1080/02693445.1879.12027958

Pérez-García A, Ortega F (2011) *Selenemys lusitanica*, gen. et sp. nov., a new pleurosternid turtle (Testudines: Paracryptodira) from the Upper Jurassic of Portugal. Journal of Vertebrate Paleontology 31(1): 60–69. https://doi.org/10.1080/02724634.2011.540054

Perrichon G, Hautier L, Pochat-Cottilloux Y, Raselli I, Salaviale C, Dailh B, Rinder N, Fernandez V, Adrien J, Lachambre J, Martin JE (2023) Ontogenetic variability of the intertympanic sinus distinguishes lineages within Crocodylia. Journal of Anatomy 242(6): 1096–1123. https://doi.org/10.1111/joa.13830

Pierce SE, Williams M, Benson RB (2017) Virtual reconstruction of the endocranial anatomy of the early Jurassic marine crocodylomorph *Pelagosaurus typus* (Thalattosuchia). PeerJ 5: e3225. https://doi.org/10.7717/peerj.3225

Platt SG, Rainwater TR, Thorbjarnarson JB, Martin D (2011) Size estimation, morphometrics, sex ratio, sexual size dimorphism, and biomass of *Crocodylus acutus* in the coastal zone of Belize. Salamandra 47(4): 179–192.

Pochat-Cottilloux Y, Martin JE, Jouve S, Perrichon G, Adrien J, Salaviale C, Muizon C, Cespedes R, Amiot R (2022) The neuroanatomy of *Zulmasuchus querejazus* (Crocodylomorpha, Sebecidae) and its implications for the paleoecology of sebecosuchians. The Anatomical Record 305(10): 2708–2728. https://doi.org/10.1002/ar.24826

Pochat-Cottilloux Y, Lauprasert K, Chanthasit P, Manitkoon S, Adrien J, Lachambre J, Amiot R, Martin JE (2024) New Cretaceous neosuchians (Crocodylomorpha) from Thailand bridge the evolutionary history of atoposaurids and paralligatorids. Zoological Journal of the Linnean Society 202(2): zlad195. https://doi.org/10.1093/zoolinnean/zlad195

Pol D, Turner AH, Norell MA (2009) Morphology of the Late Cretaceous crocodylomorph *Shamosuchus djadochtaensis* and a discussion of neosuchian phylogeny as related to the origin of Eusuchia. Bulletin of the American Museum of Natural History 2009(324): 1–103. https://doi.org/10.1206/0003-0090-324.1.1

Puértolas-Pascual E, Mateus O (2020) A three-dimensional skeleton of Goniopholididae from the Late Jurassic of Portugal: implications for the Crocodylomorpha bracing system. Zoological Journal of the Linnean Society 189(2): 521–548. https://doi.org/10.1093/zoolinnean/zlz102

Puértolas E, Canudo JI, Cruzado-Caballero P (2011) A new crocodylian from the Late Maastrichtian of Spain: implications for the initial radiation of crocodyloids. PLoS ONE 6(6): e20011. https://doi.org/10.1371/journal.pone.0020011

Puértolas-Pascual E, Canudo JI, Moreno-Azanza M (2014) The eusuchian crocodylomorph *Allodaposuchus subjuniperus* sp. nov., a new species from the latest Cretaceous (upper Maastrichtian) of Spain. Historical Biology 26(1): 91–109. https://doi.org/10.1080/08912963.2012.763034

Puértolas-Pascual E, Rabal-Garcés R, Canudo JI (2015) Exceptional crocodylomorph biodiversity of 'La Cantalera' site (lower Barremian; Lower Cretaceous) in Teruel, Spain. Palaeontologia Electronica 18: 1–16. https://doi.org/10.26879/514

Puértolas-Pascual E, Serrano-Martínez A, Pérez-Pueyo M, Bádenas B, Canudo JI (2022) New data on the neuroanatomy of basal eusuchian crocodylomorphs (Allodaposuchidae) from the Upper Cretaceous of Spain. Cretaceous Research 135: 105170. https://doi.org/10.1016/j.cretres.2022.105170

Puértolas-Pascual E, Kuzmin IT, Serrano-Martínez A, Mateus O (2023) Neuroanatomy of the crocodylomorph *Portugalosuchus azenhae* from the late Cretaceous of Portugal. Journal of Anatomy 242(6): 1146–1171. https://doi.org/10.1111/joa.13836

Ristevski J (2022) Neuroanatomy of the mekosuchine crocodylian *Trilophosuchus rackhami* Willis, 1993. Journal of Anatomy 241(4): 981–1013. https://doi.org/10.1111/joa.13732

Rotatori FM, Moreno-Azanza M, Mateus O (2022) Reappraisal and new material of the holotype of *Draconyx loureiroi* (Ornithischia: Iguanodontia) provide insights on the tempo and modo of evolution of thumb-spiked dinosaurs. Zoological Journal of the Linnean Society 195(1): 125–156. https://doi.org/10.1093/zoolinnean/zlab113

Salisbury SW, Naish D (2011) Crocodilians. In: Batten DJ (Ed.) English Wealden Fossils. The Palaeontological Association, London, 305–369.

Salisbury SW, Molnar RE, Frey E, Willis PM (2006) The origin of modern crocodyliforms: new evidence from the Cretaceous of Australia. Proceedings of the Royal Society B: Biological Sciences 273(1600): 2439–2448. https://doi.org/10.1098/rspb.2006.3613

Schwab JA, Young MT, Neenan JM, Walsh SA, Witmer LM, Herrera Y, Brusatte SL (2020) Inner ear sensory system changes as extinct crocodylomorphs transitioned from land to water. Proceedings of the National Academy of Sciences 117(19): 10422–10428. https://doi.org/10.1073/pnas.2002146117

Schwarz D (2002) A new species of *Goniopholis* from the Upper Jurassic of Portugal. Palaeontology 45(1): 185–208. https://doi.org/10.1111/1475-4983.00233

Schwarz D, Fechner R (2004) *Lusitanisuchus*, a new generic name for *Lisboasaurus mitracostatus* (Crocodylomorpha: Mesoeucrocodylia), with a description of new remains from the Upper Jurassic (Kimmeridgian) and Lower Cretaceous (Berriasian) of Portugal. Canadian Journal of Earth Sciences 41(10): 1259–1271. https://doi.org/10.1139/e04-059

Schwarz D, Salisbury SW (2005) A new species of *Theriosuchus* (Atoposauridae, Crocodylomorpha) from the late Jurassic (Kimmeridgian) of Guimarota, Portugal. Geobios 38(6): 779–802. https://doi.org/10.1016/j.geobios.2004.04.005

Schwarz D, Fechner R (2008) The first dentary of *Lisboasaurus* (Crocodylomorpha, ?Mesoeucrocodylia) from the Lower Cretaceous (Barremian) of Uña, Cuenca Province, Spain. Journal of Vertebrate Paleontology 28(1): 264–268. https://doi.org/10.1671/0272-4634(2008)28[264:TFDOLC]2.0.CO;2

Schwarz D, Raddatz M, Wings O (2017) *Knoetschkesuchus langenbergensis* gen. nov. sp. nov., a new atoposaurid crocodyliform from the Upper Jurassic Langenberg Quarry (Lower Saxony, northwestern Germany), and its relationships to *Theriosuchus*. PLoS ONE 12(2): e0160617. https://doi.org/10.1371/journal.pone.0160617

Seiffert J (1970) Oberjurassische Lazertilier aus der Kohlengrube Guimarota bei Leiria:(Mittelportugal). PhD Thesis, Freie Universität, Berlin, Germany.

Seiffert J (1973) Upper Jurassic lizards from central Portugal. Contribução para o Conhecimento da Fauna do Kimeridgiano da Mina de Lignito Guimarota (Leiria, Portugal). Memórias dos Serviços geológicos de Portugal 22: 7–85.

Sereno P, Larsson H (2009) Cretaceous crocodyliforms from the Sahara. ZooKeys 28: 1–143. https://doi.org/10.3897/zookeys.28.325

Serrano-Martínez A (2019) Análisis de la evolución neurocraneal en la radiación temprana de Eusuchia. PhD Thesis, Universidad Nacional de Educación a Distancia, UNED, Madrid, Spain.

Serrano-Martínez A, Knoll F, Narváez I, Ortega F (2019a) Brain and pneumatic cavities of the braincase of the basal alligatoroid *Diplo-*

cynodon tormis (Eocene, Spain). Journal of Vertebrate Paleontology 39(1): e1572612. https://doi.org/10.1080/02724634.2019.1572612

Serrano-Martínez A, Knoll F, Narváez I, Lautenschlager S, Ortega F (2019b) Inner skull cavities of the basal eusuchian *Lohuecosuchus megadontos* (Upper Cretaceous, Spain) and neurosensorial implications. Cretaceous Research 93: 66–77. https://doi.org/10.1016/j.cretres.2018.08.016

Serrano-Martínez A, Knoll F, Narváez I, Lautenschlager S, Ortega F (2021) Neuroanatomical and neurosensorial analysis of the Late Cretaceous basal eusuchian *Agaresuchus fontisensis* (Cuenca, Spain). Papers in Palaeontology 7(1): 641–656. https://doi.org/10.1002/spp2.1296

Serrano-Martínez A, Luján ÀH, García-Pérez Á, Fortuny J (2025) New data on the inner skull cavities of *Diplocynodon tormis* (Crocodylia, Diplocynodontinae) from the Duero Basin (Iberian Peninsula, Spain). Fossil Record 28(1): 67–77. https://doi.org/10.3897/fr.28.133743

Spiekman SN, Fernandez V, Butler RJ, Dollman KN, Maidment SC (2023) A taxonomic revision and cranial description of *Terrestrisuchus gracilis* (Archosauria, Crocodylomorpha) from the Upper Triassic of Pant-y-Ffynnon Quarry (southern Wales). Papers in Palaeontology 9(6): e1534. https://doi.org/10.1002/spp2.1534

Spoor F, Bajpai S, Hussain ST, Kumar K, Thewissen JG (2002) Vestibular evidence for the evolution of aquatic behaviour in early cetaceans. Nature 417(6885): 163–166. https://doi.org/10.1038/417163a

Taylor AM, Gowland S, Leary S, Keogh KJ, Martinius AW (2014) Stratigraphical correlation of the Late Jurassic Lourinhã Formation in the Consolação Sub-basin (Lusitanian Basin), Portugal. Geological Journal 49(2): 143–162. https://doi.org/10.1002/gj.2505

Tennant JP, Mannion PD, Upchurch P (2016) Evolutionary relationships and systematics of Atoposauridae (Crocodylomorpha: Neosuchia): implications for the rise of Eusuchia. Zoological Journal of the Linnean Society 177(4): 854–936. https://doi.org/10.1111/zoj.12400

Tucker AS (2017) Major evolutionary transitions and innovations: the tympanic middle ear. Philosophical Transactions of the Royal Society B: Biological Sciences 372(1713): 20150483. https://doi.org/10.1098/rstb.2015.0483

Turner AH (2015) A review of *Shamosuchus* and *Paralligator* (Crocodyliformes, Neosuchia) from the Cretaceous of Asia. PLoS ONE 10(2): e0118116. https://doi.org/10.1371/journal.pone.0118116

Turner AH, Buckley GA (2008) *Mahajangasuchus insignis* (Crocodyliformes: Mesoeucrocodylia) cranial anatomy and new data on the origin of the eusuchian-style palate. Journal of Vertebrate Paleontology 28(2): 382–408. https://doi.org/10.1671/0272-4634(2008)28[382:MICMCA]2.0.CO;2

Turner AH, Pritchard AC (2015) The monophyly of Susisuchidae (Crocodyliformes) and its phylogenetic placement in Neosuchia. PeerJ 3: e759. https://doi.org/10.7717/peerj.759

Venczel M, Codrea VA (2019) A new *Theriosuchus*-like crocodyliform from the Maastrichtian of Romania. Cretaceous Research 100: 24–38. https://doi.org/10.1016/j.cretres.2019.03.018

Vidal LM (1915) Nota geológica y paleontológica sobre el Jurásico superior de la provincia de Lérida. Boletín del Instituto Geológico de España 16: 17–55.

Walsh SA, Barrett PM, Milner AC, Manley G, Witmer LM (2009) Inner ear anatomy is a proxy for deducing auditory capability and behaviour in reptiles and birds. Proceedings of the Royal Society B: Biological Sciences 276(1660): 1355–1360. https://doi.org/10.1098/rspb.2008.1390

Walker AD (1970) A revision of the Jurassic reptile *Hallopus victor* (Marsh), with remarks on the classification of crocodiles. Philosophical Transactions of the Royal Society of London B, Biological Sciences 257(816): 323–372. https://doi.org/10.1098/rstb.1970.0028

Webb GJW, Messel H (1978) Morphometric analysis of *Crocodylus porosus* from the north coast of Arnhem Land, northern Australia. Australian Journal of Zoology 26(1): 1–27. https://doi.org/10.1071/ZO9780001

Wellnhofer P (1971) Die Atoposauridae (Crocodylia, Mesosuchia) der Oberjura-Plattenkalke Bayerns. Palaeontographica Abteilung A 138: 133–165.

Whetstone K, Whybrow P (1983) A "cursorial" crocodilian from the Triassic of Lesotho (Basutoland), southern Africa. Occasional Papers of the University of Kansas Museum of Natural History 106: 1–37.

Wilberg EW, Beyl AR, Pierce SE, Turner AH (2022) Cranial and endocranial anatomy of a three-dimensionally preserved teleosauroid thalattosuchian skull. The Anatomical Record 305(10): 2620–2653. https://doi.org/10.1002/ar.24704

Wilson RCL, Hiscott RN, Willis MG, Gradstein FM (1989) The Lusitanian Basin of West-central Portugal: Mesozoic and Tertiary tectonic, stratigraphic and subsidence history. In: Tankard AJ, Balkwill HR (Eds) Extensional tectonics and stratigraphy of the North Atlantic margins. AAPG Memoir 46: 341–361. https://doi.org/10.1306/M46497C22

Witmer LM, Ridgely RC (2009) New insights into the brain, braincase, and ear region of tyrannosaurs (Dinosauria, Theropoda), with implications for sensory organization and behavior. The Anatomical Record 292(9): 1266–1296. https://doi.org/10.1002/ar.20983

Witmer LM, Ridgely RC, Dufeau DL, Semones MC (2008) Using CT to peer into the past: 3D visualization of the brain and ear regions of birds, crocodiles, and nonavian dinosaurs. In: Endo H, Frey R (Eds) Anatomical imaging: towards a new morphology. Springer, Tokyo Berlin, Heidelberg, New York, 67–87. https://doi.org/10.1007/978-4-431-76933-0_6

Woodward AS (1896) On two Mesozoic crocodilians *Notosuchus* (genus novum) and *Cynodontosuchus* (genus novum) from the Red Sandstones of the Territory of Neuquén (Argentina Republic). Anales del Museo de La Plata, Paleontología 4: 1–20.

Wu XC, Russell AP, Brinkman DB (2001) A review of *Leidyosuchus canadensis* Lambe, 1907 (Archosauria: Crocodylia) and an assessment of cranial variation based upon new material. Canadian Journal of Earth Sciences 38(12): 1665–1687. https://doi.org/10.1139/e01-059

Young MT, Hua S, Steel L, Foffa D, Brusatte SL, Thüring S, Mateus O, Ruiz-Omeñaca JI, Havlik P, Lepage Y, de Andrade MB (2014) Revision of the late Jurassic teleosaurid genus Machimosaurus (Crocodylomorpha, Thalattosuchia). Royal Society Open Science 1(2): 140222. https://doi.org/10.1098/rsos.140222

Supplementary material 1

Matrix + Consensus

Author: E. Puértolas-Pascual

Data type: nex

Link: https://doi.org/10.3897/fr.28.167846.suppl1

Supplementary material 2

Cladogram

Author: E. Puértolas-Pascual
Data type: pdf
Explanation note: Phylogenetic relationships showing the position of ML2631. Analysis based on the matrix of Pochat-Cottilloux et al. (2024). Time-calibrated strict consensus tree.

Link: https://doi.org/10.3897/fr.28.167846.suppl2

Supplementary material 3

3D models and cavities

Author: E. Puértolas-Pascual
Data type: zip
Explanation note: Part 01–04 of the compressed skull model of ML2631. Cavities models of ML2631.

Link: https://doi.org/10.3897/fr.28.167846.suppl3